Accepted Manuscript

Urea-containing peptide boronic acids as potent proteasome inhibitors

Li-Qiang Han, Xia Yuan, Xing-Yu Wu, Ri-Dong Li, Bo Xu, Qing Cheng, Zhen-Ming Liu, Tian-Yan Zhou, Hao-Yun An, Xin Wang, Tie-Ming Cheng, Ze-Mei Ge, Jing-Rong Cui, Run-Tao Li

PII: S0223-5234(16)30886-8

DOI: 10.1016/j.ejmech.2016.10.023

Reference: EJMECH 8988

To appear in: *European Journal of Medicinal Chemistry*

Received Date: 3 August 2016

Revised Date: 9 October 2016

Accepted Date: 12 October 2016

Please cite this article as: L.-Q. Han, X. Yuan, X.-Y. Wu, R.-D. Li, B. Xu, Q. Cheng, Z.-M. Liu, T.-Y. Zhou, H.-Y. An, X. Wang, T.-M. Cheng, Z.-M. Ge, J.-R. Cui, R.-T. Li, Urea-containing peptide boronic acids as potent proteasome inhibitors, *European Journal of Medicinal Chemistry* (2016), doi: 10.1016/j.ejmech.2016.10.023.

This is a PDF file of an unedited manuscript that has been accepted for publication. As a service to our customers we are providing this early version of the manuscript. The manuscript will undergo copyediting, typesetting, and review of the resulting proof before it is published in its final form. Please note that during the production process errors may be discovered which could affect the content, and all legal disclaimers that apply to the journal pertain.

Graphical abstract

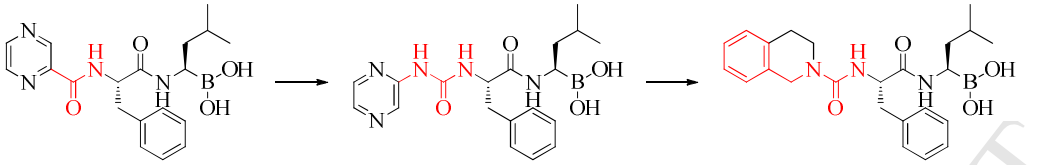

CT-L activity: IC_{50} = 4.0 nM

Bortezomib

CT-L activity: IC_{50} = 0.2 pM

4 Cell lines growth: IC_{50} < 10 nM

I-14

ACCEPTED MANUSCRIPT

ACCEPTED MANUSCRIPT

Urea-containing peptide boronic acids as potent proteasome inhibitors

Li-Qiang Han [a], Xia Yuan [a], Xing-Yu Wu [a], Ri-Dong Li [a], Bo Xu [a], Qing Cheng [a], Zhen-Ming Liu [a], Tian-Yan Zhou [a], Hao-Yun An [b], Xin Wang [a], Tie-Ming Cheng [a], Ze-Mei Ge [a,*], Jing-Rong Cui [a,*], Run-Tao Li [a,*]

[a] *State Key Laboratory of Natural and Biomimetic Drugs, School of Pharmaceutical Sciences, Peking University, Beijing 100191, PR China*

[b] *Zhengzhou Granlen PharmaTech, Ltd. 1300 East Hanghai Road, Zhengzhou, Henan 450016, PR China*

Abstract

A novel class of urea-containing peptide boronic acids as proteasome inhibitors was designed by introducing a urea scaffold to replace an amido bond. Compounds were synthesized and their antitumor activities were evaluated. After two rounds of optimizations, the compound **I-14** was found to be a potent proteasome inhibitor. Compared with Bortezomib, **I-14** showed higher potency against the chymotrypsin-like activity of human 20S proteasome (IC_{50} < 1 pM), similar potency against four different cancer cell lines (IC_{50} < 10 nM), and better pharmacokinetic profile. Furthermore, **I-14** significantly inhibited tumor growth in Bel7404 mouse xenograft model. The excellent proteasome inhibition by **I-14** was rationalized through docking and molecular dynamics studies.

Keywords:
Urea-containing peptide boronic acids; Proteasome inhibitor; Anti-tumor activity; Structure-activity relationship; Low toxicity

1. Introduction

Proteasome is the most abundant and ubiquitous enzymatic complex responsible for intracellular protein turnover in eukaryotic cells [1]. Its substrates include a large variety of cell proteins that control apoptosis, cell-cycle progression, DNA repair and many other cellular regulatory mechanisms [2], and therefore it plays an important role in the regulation of many physiological processes as well as in the development of a number of major human diseases. The catalytic core particle of the 20S proteasome has become a major target for anticancer and anti-autoimmune drugs [3]. The peptide boronate Bortezomib (Velcade®) is the first 20S proteasome inhibitor entering clinical practice, approved by FDA for treating multiple myeloma in 2003 and mantle cell lymphoma in 2006 [4]. Since then, a series of proteasome inhibitors have advanced to clinic or clinical trials, including peptide boronic acids

*Corresponding author. Tel./fax: +86 10 82805954.
E-mail address: lirt@bjmu.edu.cn (R.-T. Li), zmge@bjmu.edu.cn (Z.-M. Ge), jrcui@bjmu.edu.cn (J.-R. Cui)

(Delanzomib, CEP-18770) [5], epoxyketones (Carfilzomib, approved in July 2012 for treating multiple myeloma) [6], β-lactones such as NPI-0052 (Marizomib) [7], *etc.* (Fig. 1). Although peptide boronic acids are one of the most important chemical classes of proteasome inhibitors, most of them have poor pharmacokinetic properties, which greatly limited their clinical applications [8]. Even for Bortezomib, after bolus *i.v.* administration at 0.8 mg/kg, the mean half-life, the mean apparent volume of distribution (Vd) and the plasma clearance rate (CL) were only 0.8 ± 0.1 h, 2.4 ± 0.8 L/kg and 34 ± 11 mL/min/kg, respectively [9], and in the initial pharmacokinetic studies, it was found to be rapidly metabolized in the plasma compartment (>90% is cleared within 15 minutes of *i.v.* administration) [10]. These results could be partly attributed to the instability of the peptide bonds in the molecule [11]. However, to date, current efforts in improving peptide boronic acid proteasome inhibitors mostly focus on the modifying the amino acid residues and the N-end substituents [12-17], but rarely changing the amido bonds.

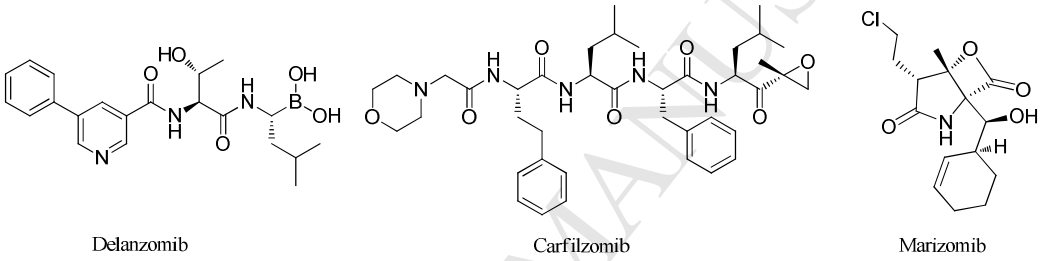

Fig 1. Structures of Delanzomib, Carfilzomib and Marizomib

Replacing the amido bond in the peptide with the urea framework is a common strategy known to improve the PK/PD properties of peptide drugs. Besides, the urea scaffold has been exploited in several other classes of proteasome inhibitors (Fig. 2) [18-20].

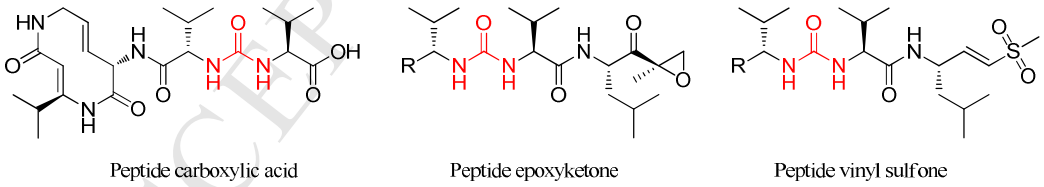

Fig 2. Reported peptide inhibitors containing the urea scaffold.

Inspired by this, we designed and synthesized a novel class of urea-containing peptide boronic acids as proteasome inhibitors, which have both the urea scaffold and peptide boronic acid as warheads. Further optimization led to the discovery of a potent proteasome inhibitor **I-14** with excellent *in vitro* and *in vivo* antitumor activities, low toxicity and good pharmacokinetic properties.

2. Results and discussion

2.1. Design, synthesis and biological activities of first-round compounds

Our initial studies started by examining the influence of distance between the urea segment and the boronic acid group. We designed two series of compounds with urea segment away from (**I**) and next to (**II**) the boron acid group (Fig. 3), in which n = 0 represents dipeptides and n = 1 represents tripeptides, respectively. **R_1, R_2** and **R_3** are chosen from the corresponding groups in known effective peptide boronic acid proteasome inhibitors.

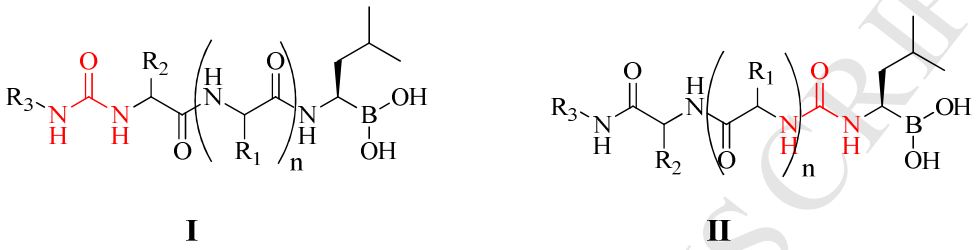

I **II**

Fig 3. Structures of compounds **I** and **II**

The synthetic routes of the two series of compounds are illustrated in Scheme 1 using **I-1** and **II-1** as examples. Because peptide boronic acids are difficult to purify and α-amido boronic acid is the most expensive among all intermediates, the α-amido boronic acid segment was attached only in the last step. The key urea scaffold was introduced based on literature method with modification [21]. For the synthesis of **I-1**, benzylamine and L-phenylalanine methyl ester hydrochloride were reacted with 1,1-carbonyldiimidazole (CDI) to form the urea part **I-1a** in 87% yield. **I-1a** was further treated with NaOH and then with HCl to give the corresponding hydrolyzed product **I-1b**. In the presence of dicyclohexylcarbodiimide (DCC) and *N*-hydroxybenzotriazole (HOBt), **I-1b** was coupled with α-amino boronic acid pinacol ester, which was synthesized according to Ellman's procedure [22], to provide key intermediate urea-containing peptide boronic acid pinacol ester **I-1c**. The target compound **I-1** was obtained after the pinacol protecting group of **I-1c** was removed using a novel method developed by Santos and coworkers [23]. For the synthesis of compound **II-1**, the starting material *N*-Boc-L-phenylalanine was first condensed with 4-methoxybenzylamine in the presence of DCC and HOBt to give the protected intermediate **II-1a**, which was treated with HCl to generate the corresponding deprotected product **II-1b**. The crude **II-1b** was coupled with α-amino boronic acid pinacol ester by the same method as described above for **I-1a** to give the urea-containing peptide boronic acid pinacol ester **II-1c**. Finally, the pinacolyl protecting group of **II-1c** was removed using the same procedure as used for obtaining **I-1** to provide the free boronic acid **II-1**.

Compounds **I-2~I-10** and **II-2~II-7** were synthesized similarly through the same procedures. All key intermediates and final products were characterized by ^{1}H NMR, ^{13}C NMR and MS.

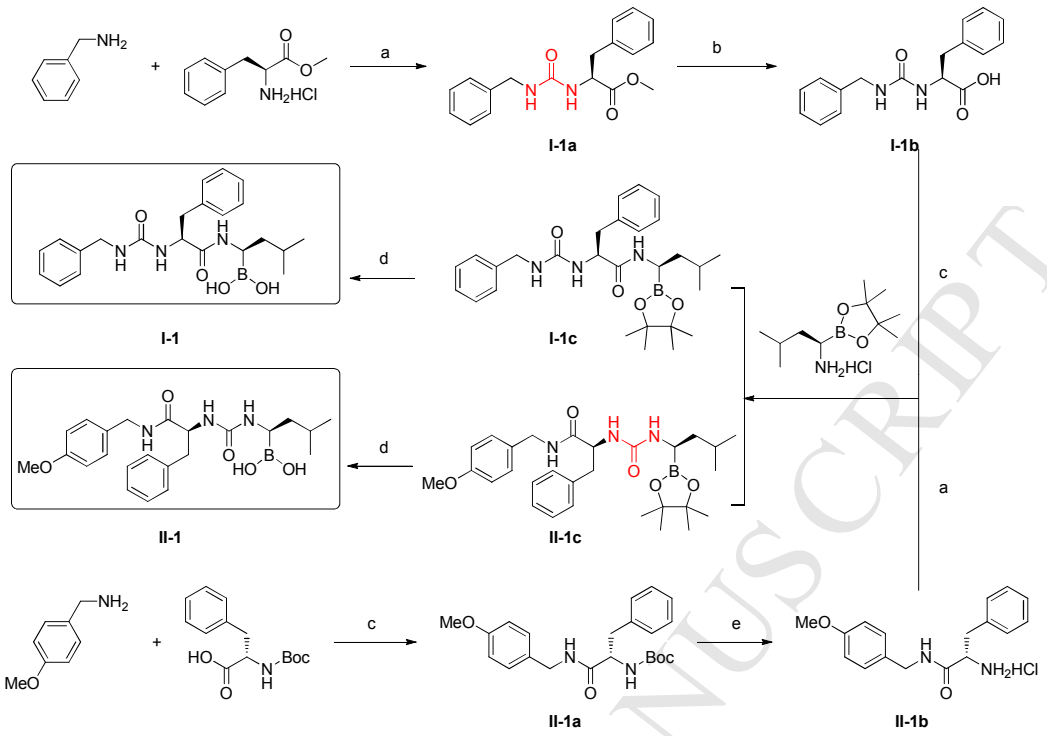

Scheme 1. Synthesis of target compounds **I-1** and **II-1**. Reagents and conditions: (a) CDI, DMF, MeCN, rt; (b) i. NaOH, 0°C; ii. HCl, 0°C; (c) DCC, HOBt, DIEA, CH_2Cl_2, rt; (d) i. DEA (Diethanolamine), EtOAc, rt; ii. HCl, H_2O, EtOAc, rt; (e) 10 M HCl in EtOH, CH_2Cl_2.

The inhibitory effects of the **I-1~I-10** and **II-1~II-7** on the chymotrypsin-like (ChT-L), caspase-like (C-L), and trypsin-like (T-L) activities of human 20S proteasome were measured at 0.2 μM and 2 μM using Bortezomib as the positive control. The results are summarized in Table 1. It is clear that the series **I** compounds (urea moiety away from boron atom) are more potent in inhibiting ChT-L activity than the series **II** compounds (urea moiety next to boron atom). The lower potency of series **II** compounds can be ascribed to the tautomeric interconversion shown in Scheme 2. Due to the strong electrophilicity of the boron atom, a five-member ring is easily formed through a coordination bond and then one molecule of water is eliminated [24]. This speculation is supported by the ESI results of the series **II** compounds, which mainly give the $[M\text{-}17]^+$ peaks (i.e., $[M-H_2O+1]^+$, see Supplementary Material, Figure S1). Comparing the activities of compounds **I-3** with **I-9**, and **II-3** with **II-7** shows that tripeptide analogues are obviously better than dipeptide analogues, which is consistent with our previous report [14]. Interestingly, compound **II-5** with the unnatural D-amino acid does not show distinct difference from the corresponding its L-configuration amino acid compounds analogue **II-3**. In addition, I-6 and I-10 have equal potency against ChT-L compared with Bortezomib. However, they are ineffective or less potent than Bortezomib against C-L and T-L, suggesting that they are effective and selective proteasome inhibitors. More interestingly, compounds (**I-1, I-2, I-5** and **I-6**) that have benzyl or substituted benzyl group as $\mathbf{R_1}$ exhibited more potent anti-proteasome activity than other compounds.

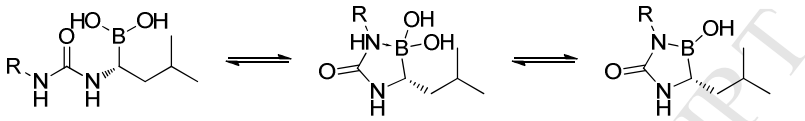

Scheme 2. Predicted interconversion of compounds in series **II**

Table 1

General structures and biological activity of target compounds (% inhibition).

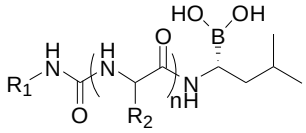

I

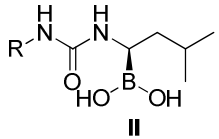

II

Comp. No.	n	R_1	R_2	R	ChT-L		C-L		T-L	
					0.2 μM	2 μM	0.2 μM	2 μM	0.2 μM	2 μM
I-1	1	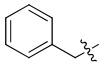	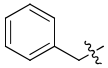		82.082	96.113	6.461	84.58	5.043	57.790
I-2	1	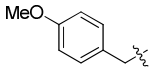	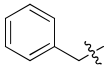		86.338	95.861	8.450	89.392	5.722	53.491
I-3	1	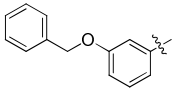	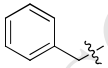		-14.639	86.614	-14.446	-2.926	-2.888	12.266
I-4	1		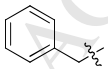		10.548	87.304	3.748	8.575	-3.766	10.537

ACCEPTED MANUSCRIPT

I-5	1	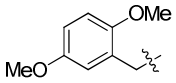	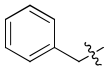	82.067	96.655	9.814	68.776	4.990	56.881
I-6	1	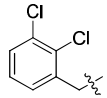	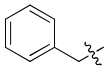	91.940	96.544	-23.048	-26.615	35.572	83.660
I-7	1	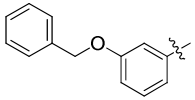	-H	47.308	90.946	8.577	62.467	0.355	29.284
I-8	1	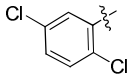	-H	61.963	89.674	10.065	7.173	-3.948	28.328
I-9	2	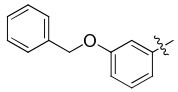	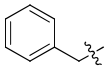	49.489	90.992	-13.661	-20.492	-0.748	47.155
I-10	1	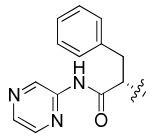	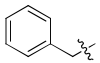	84.643	95.724	-21.838	-24.724	-0.926	43.457
II-1	1		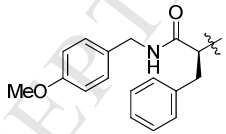	33.819	86.790	40.869	87.942	-6.549	22.848
II-2	1		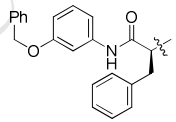	-14.170	10.372	2.030	2.190	6.916	4.381

ACCEPTED MANUSCRIPT

II-3	1	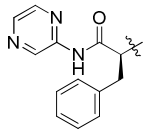	-0.670	44.666	17.405	66.342	-3.924	2.409
II-4	1	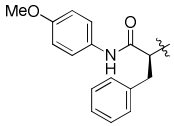	2.873	59.740	1.617	7.355	-1.392	9.321
II-5	1	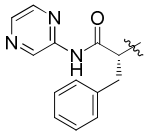	-4.193	47.804	18.952	79.767	-12.27	-5.926
II-6	1	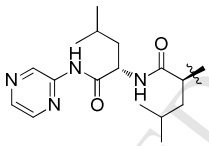	5.785	52.830	12.760	32.649	-8.060	-5.632
II-7	1	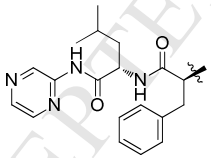	63.305	93.361	9.760	73.204	-7.933	34.743
Bortezomib			91.554		55.563		33.278	

ACCEPTED MANUSCRIPT

2.2. Design, synthesis and biological activities of second-round compounds

The first round showed that series **I** compounds (urea away from boronic acid) were much more potent than series **II** compounds (urea next to boronic acid) and it is preferable to have a benzyl group at the N-terminal. Thus, we next focused our attention on the optimization of the benzyl group at the N-terminal in series **I** compounds. A series of new analogues were designed and synthesized through the same methodology described above, except that compound **I-24** was a side product [25] obtained during the preparation of **I-14**. All these second-round compounds **I-11~I-24** were evaluated for their proteasome inhibitory activity against ChT-L and their potency against the hepatocellular carcinoma HepG-2 and human gastric cancer MGC-803 cell lines. The structures and results are listed in Table 2.

Table 2.

Structure and biological activity (IC_{50} in nM) of second-round compounds.

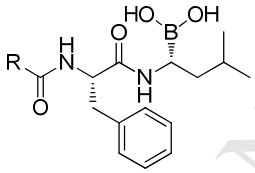

Comp. No.	R	ChT-L	HepG-2	MGC-803
I-1	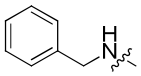	10 ± 3	87.25 ± 14	18.76 ± 7
I-11	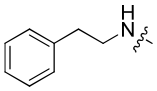	20 ± 0.6	70.86 ± 9	30.01 ± 6
I-12	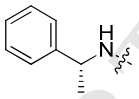	10 ± 1	36.99 ± 4	4.084 ± 1
I-13	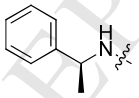	200 ± 20	1072 ± 161	198.2 ± 14
I-14	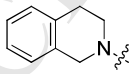	0.0002 ± 0.0001	19.38 ± 3	3.962 ± 1
I-15	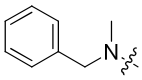	2 ± 0.8	30.49 ± 2	5.203 ± 1
I-16	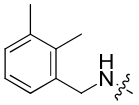	4 ± 2	44.68 ± 3	6.298 ± 1
I-17	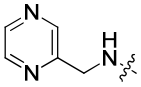	50 ± 6	4136 ± 479	738.2 ± 111

I-18	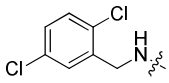	40 ± 3	70.67 ± 14	28.87 ± 8
I-19	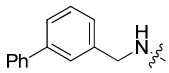	0.3 ± 0.07	37.25 ± 1	5.873 ± 1
I-20	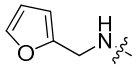	20 ± 10	45.60 ± 2	5.316 ± 2
I-21	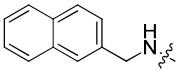	12 ± 1	53.08 ± 14	7.062 ± 0
I-22	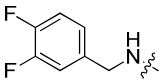	2 ± 0.9	38.82 ± 1	6.698 ± 0
I-23	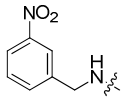	3 ± 1	43.81 ± 3	6.317 ± 0
I-24	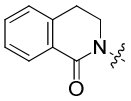	660 ± 70	59.67 ± 4	7.298 ± 0
Bortezomib		4 ± 0.3	36.57 ± 3	5.782 ± 0

As shown in Table 2, all tested compounds exhibited excellent ChT-L inhibitory activity (IC_{50} varying from <1 nM to 50 nM) except the benzylic methyl substituted compound **I-13** and the benzylic oxidized derivative **I-24**. In particular, compound **I-14** reached an IC_{50} of 0.0002 nM against ChT-L, which is much more potent than Bortezomib (IC_{50} = 4.0 nM). Extending the benzyl amino (**I-1**) to phenylethyl amino (**I-11**) did not significantly improve the ChT-L inhibitory activity. Compounds **I-12** (IC_{50} = 10 nM) and **I-13** (IC_{50} = 200 nM) both introduced a methyl group at the methylene position in **I-1** but showed 20 times difference in their activity against ChT-L, suggesting that the chiral center can greatly influence the activity. However, we did not further optimize the substituents at methylene position of compound **I-1**, since neither **I-12** nor **I-13** was significantly better than **I-1**. The N-methyl substituted derivative **I-15** (IC_{50} = 2 nM) and the cyclized 1,2,3,4-tetrahydroisoquinoline derivative **I-14** (IC_{50} = 0.0002 nM) showed very strong inhibitory activity against ChT-L proteasome, indicating that replacing the hydrogen in the amino group with an alkyl group is favorable, and restricting the conformation of the amine also helps greatly. The type and position of substituents on the phenyl ring of the benzylamino group obviously can affect the activity. For example, **I-18** (2,5-dichloro, IC_{50} = 40 nM) showed 15–20 times weaker potency in ChT-L inhibition than **I-16** (2,3-dimethyl, IC_{50} = 4 nM), **I-22** (3,4-difluoro, IC_{50} = 2 nM) and **I-23** (3-nitro, IC_{50} = 3 nM). More notably, the 3-phenyl analogue **I-19** showed exceptional ChT-L inhibitory activity (IC_{50} = 0.3 nM), suggesting that the aryl substituent is more favorable than others. However, using other aromatic moieties such as naphthyl (**I-21**), pyrazinyl (**I-17**) and furanyl (**I-20**) groups in the place of the phenyl ring of the benzylamino group in **I-1**

ACCEPTED MANUSCRIPT

did not improve the resulting compounds' potency on inhibiting ChT-L activity.

In addition, all compounds except **I-13** and **I-17** also produced excellent potency against HepG-2 and MGC-803 cells lines (IC_{50} < 100 nM), among which four compounds (**I-12**, **I-14**, **I-15** and **I-19**) had comparable or higher potency than Bortezomib. The most potent compound was still **I-14**. The diastereoisomers **I-12** (HepG-2, IC_{50} = 39.99 nM; MGC-803, IC_{50} = 14.084 nM) and **I-13** (HepG-2, IC_{50} = 1072 nM; MGC-803, IC_{50} = 198.2 nM) again had dramatically different potency, further illustrating the importance of chirality on that benzylic position. Note that **I-24** had satisfying potency against both cancer cell lines but fell short to effectively suppress proteasome ChT-L activity. The rationale behind this phenomenon is under further investigation due to the novel structure of **I-24**.

Based on the above results, three potential compounds (**I-6**, **I-14** and **I-22**) were selected to be tested further against 11 human tumor cell lines using Bortezomib (**PS-341**) as the positive control. The results are summarized in **Table 3**.

Table 3.

Biological results of three compounds over 11 human tumor cell lines (IC_{50} in nM) [a]

No.	Cell line	Source	**I-6**	**I-14**	**I-22**	PS-341
1	A549	Lung cancer	1022.61 ± 265.45	3826.15 ± 796.42	1317.50 ± 15.43	2135.73 ± 463.00
2	95D	Lung cancer	40.96 ± 0.43	37.11 ± 0.10	58.85 ± 7.59	38.18 ± 2.39
3	HCT116	Colon cancer	23.02 ± 0.16	7.32 ± 0.79	16.07 ± 3.05	1.40 ± 0.17
4	HL-60	Leukemia	26.96 ± 1.85	7.71 ± 0.01	28.53 ± 2.03	7.60 ± 0.53
5	MGC803	Gastric cancer	17.52 ± 2.14	4.98 ± 0.06	16.73 ± 0.13	6.54 ± 0.18
6	BEL7404	Hepatoma	42.23 ± 1.65	13.75 ± 1.09	47.26 ± 0.78	25.04 ± 1.76
7	MKN45	Gastric cancer	20.11 ± 1.40	15.52 ± 2.54	26.62 ± 0.25	7.15 ± 0.41
8	SKOV3	Ovarian cancer	46.30 ± 7.32	25.88 ± 9.60	10.47 ± 3.62	1.62 ± 0.97
9	MDA-MB-231	Breast cancer	25.08 ± 1.36	17.74 ± 1.02	28.40 ± 2.49	16.65 ± 0.67
10	HepG2	Hepatocellular carcinoma	25.96 ± 5.52	8.38 ± 0.78	19.04 ± 1.90	1.61 ± 0.17
11	SW1990	Pancreatic carcinoma	80.33 ± 7.92	89.34 ± 4.51	90.73 ± 3.03	79.06 ± 2.32

[a] IC_{50} was measured over 6 concentrations based on three experiments.

Table 3 shows that all three compounds strongly inhibited the growth all tested tumor cell lines (except A549) at IC_{50} < 100 nM. In particular, **I-14** reached IC_{50} < 10 nM in four cell lines, making it comparable to Bortezomib. The three candidate compounds and Bortezomib all showed inadequate potency to the A549 cell line than to the other ten cell lines: their IC_{50} values were all 10–2000 times greater for A549 than for others. The bonoric acid is thus a selective anticancer agent.

2.3. Pharmacokinetics study of I-14

Given that the majority of currently available proteasome inhibitors containing peptide backbones are prone to rapid *in vivo* inactivation [26], we next examined

whether the urea scaffold-based proteasome inhibitor **I-14** is metabolically more stable than those peptide-based drugs. Thus, we tested the pharmacokinetics of **I-14** in three rats. The observed plasma concentration–time profile after a single *i.v.* dose of 3 mg/kg in male Sprague–Dawley rats is shown in **Fig. 4** and the main pharmacokinetic parameters estimated by WinNolin are summarized in **Table 4**, in which the half-life ($\mathbf{t_{1/2}}$) of **I-14** is 1.96 ± 0.07 h. In contrast, it was reported that after bolus *i.v.* administration of Bortezomib at 0.8 mg/kg, the mean half-life was 0.8 ± 0.1 h,[10] which is much shorter than that of **I-14**. At the same time, the mean volume of distribution (Vd) of Bortezomib was 2.4 ± 0.8 L/kg, and we can infer that the long elimination phase half-life of **I-14** is in part due to a larger volume of distribution, Vd = 9.44 ± 1.21 L/kg. These results indicate that **I-14** is more likely to have higher *in vivo* stability than Bortezomib, as the latter is known to undergo rapid metabolic inactivation [11, 27, 28].

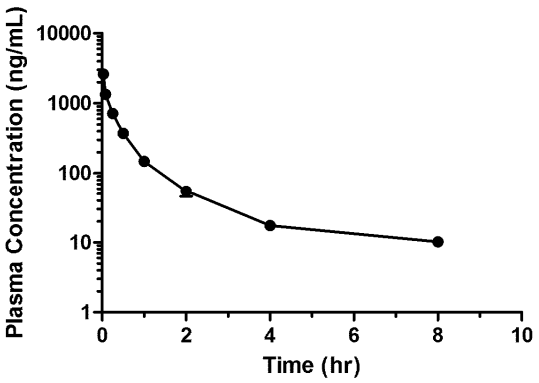

Fig 4. The plasma concentration-time curve of **I-14** in male SD rats following bolus *i.v.* administration at a dose of 3 mg/kg (n=3). Data are mean ± SD.

Table 4

Pharmacokinetic parameters of **I-14** in Rats after a bolus *i.v.* dose of 3 mg/kg (n=3)

Animal	Rat 1	Rat 2	Rat 3	Mean	SD
$t_{1/2}$ (hr)	1.93	2.04	1.91	1.96	0.07
AUC_{last} (hr*ng/mL)	958	788	887	878	85
Vd (L/kg)	8.45	10.8	9.07	9.44	1.21
CL (mL/min/kg)	50.5	61.2	54.8	55.5	5.4

2.4. In vivo anticancer activity of I-14

To assess the *in vivo* antitumor efficacy of compound **I-14**, a Bel7404 xenograft nude mice model was established, with Bortezomib (**PS-341**) as positive drug. Compound **I-14** was administered at 1 mg/kg i.v. every two days for 24 consecutive days. As shown in Fig. 5A, **I-14** could effectively suppress tumor growth, which is equivalent to Bortezomib (0.5 mg/kg). Gratifyingly, the average body weight of the

mice in the **I-14** treatment group did not drop significantly, whereas the group treated with Bortezomib showed a 10.7% loss of body weight, and even two mice died on day 20 and 24 respectively. These results revealed that **I-14** is an efficient anticancer agent with relatively low toxicity.

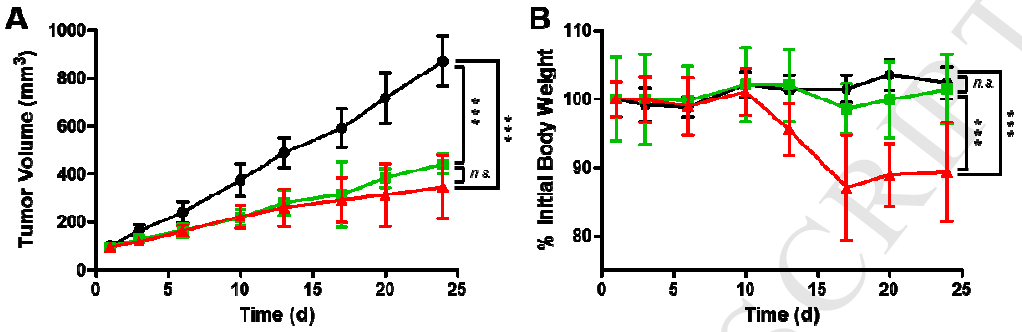

Figure 5. **I-14** inhibits tumor growth *in vivo* at 1 mg/kg. (A) Tumor growth curves in mice receiving the respective treatments by tumor volume (Black: control, n = 8; Green: **I-14** 1 mg/kg *i.v.* qod, n = 6; Red: Bortezomib 0.5 mg/kg *i.v.* qod, n = 6). (B) Average body weight of mice (percentage of initial) receiving the respective treatments surviving on a given day. The results are represented as means ± SD and analyzed by two-way ANOVA. *n.s.* non-significant, *** P<0.001.

2.5. Docking and molecular dynamics study of I-14

To understand the binding profile and account for the superior bioactivity of **I-14** than **PS-341**, we performed a molecular docking study via Gold (Cambridge Crystallographic Data Centre) and assessed the results by Maestro (Schrödinger LLC.). The gene sequence of the chymotrypsin active site of the yeast 20S proteasome is highly homologous to that of the human 20S proteasome. The best binding conformation of **PS-341** has a RMSD of 1.0 Å with its original crystallized conformation.

The binding profile of **I-14** in the β5 and β6 subunit inhibitor pocket of the proteasome is depicted in Fig. 6A,B. From both the 2D binding and the Poisson–Boltzmann electrostatic surface plot, it is obvious that **I-14** closely resembled **PS-341** with its peptidomimetic chain, making essential hydrogen bonds with the receptor and fulfilling its promise as a potent proteasome inhibitor on enzymatic, cellular and animal model aspects. From the overall docking results, **I-14**, with a fitness score of 51.03, is better than **PS-341**, which scored 46.37. This is mainly due to **I-14**'s higher van der Waals interaction score (**I-14**: 41.81, **PS-341**: 36.48) together with less score penalty from internal torsion energy (−3.02 vs. −3.34) and covalent binding energy (−10.90 vs. −11.63). Indeed, the induction of the aromatic ring could contribute to the binding affinity, as there are more hydrophobic residues located around the 1,2,3,4-tetrahydroisoquinolin fragment. Meanwhile, the phenyl group in **I-14** rotated slightly and occupied the S2 subsite better than that of **PS-341** (Fig. 6B).

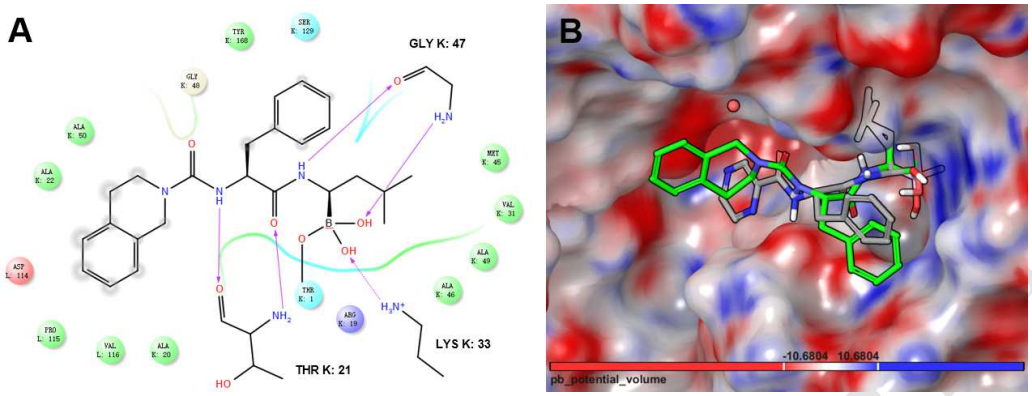

Fig. 6. Docked binding profile of **I-14** and PS-341 within the β5 and β6 subunit inhibitor pocket of yeast 20S proteasome. (A) 2D binding plot: Purple arrows and colored curves indicate hydrogen bondings and hydrophobic interactions respectively. (B) Poisson-Boltzmann electrostatic surface plot: PS-341 in its crystallized bioactive conformation is shown in grey sticks, best binding conformation of **I-14** is displayed in green, oxygen atom from the crystallized water molecule is depicted in red dot.

However, the docking results are not enough to illuminate how and why **I-14** outperformed **PS-341** on the enzymatic assay. We thus utilized Desmond to conduct a 30 ns unrestrained molecular dynamics simulation to find out. The RMSD plot of the heavy atoms throughout the simulation is shown in Fig. 7A. The trajectory is stable from 10 ns onward in accordance with the energy terms and the geometry. A representative conformation (RC) from 10 to 30 ns and the last frame (LF) were obtained as depicted in Fig. 7C. The essential hydrogen bonding derived from the docking conformation was retained throughout the simulation, although the hydrogen bonding tended to be more frequent after 10 ns (Fig. 7B, Supplementary Material, Fig. S2 B,D,E). Among the most significant increases are **I-14**-NH15 to K:GLY47 (from 40% in first 10 ns to 98% in 10–30 ns) and K:ALA49 to **I-14**-O19 (from 76% to 95%). Two new pairs of water bridge hydrogen bonding also happen in 37% of the time during the equilibrium.

The non-bonding fragments of the molecule fits the pocket better after 10 ns, leading to an increase of the binding free energy (ΔG_{bind}) of separate parts (**Figure 7D**). During the first 7 ns, we could see that the 1,2,3,4-tetrahydroisoquinolin fragment of **I-14** was gradually engulfed by the pocket and then stabilized over the final stage of the simulation, which is a distinct induced-fit effect that we were expecting. This phenomenon could help to diminish the fragment's solvent exposure (**Figure 6B, 7C**), which potentiates its van der Waals interaction, hydrophobic interaction and steric hindrance, and thus contributes to its total ΔG_{bind}.

In conclusion, the peptidomimetic chain of **I-14** highly mimicked that of **PS-341**. The receptor and the 1,2,3,4-tetrahydro-isoquinolin fragment of **I-14** underwent a induced-fit effect at the initial stage of the simulation, and whole molecule fit and interacted with the receptor better as the simulation proceeded. This can help in explaining the superior activity of **I-14** on the enzymatic aspect, confirming its potential as a promising drug candidate.

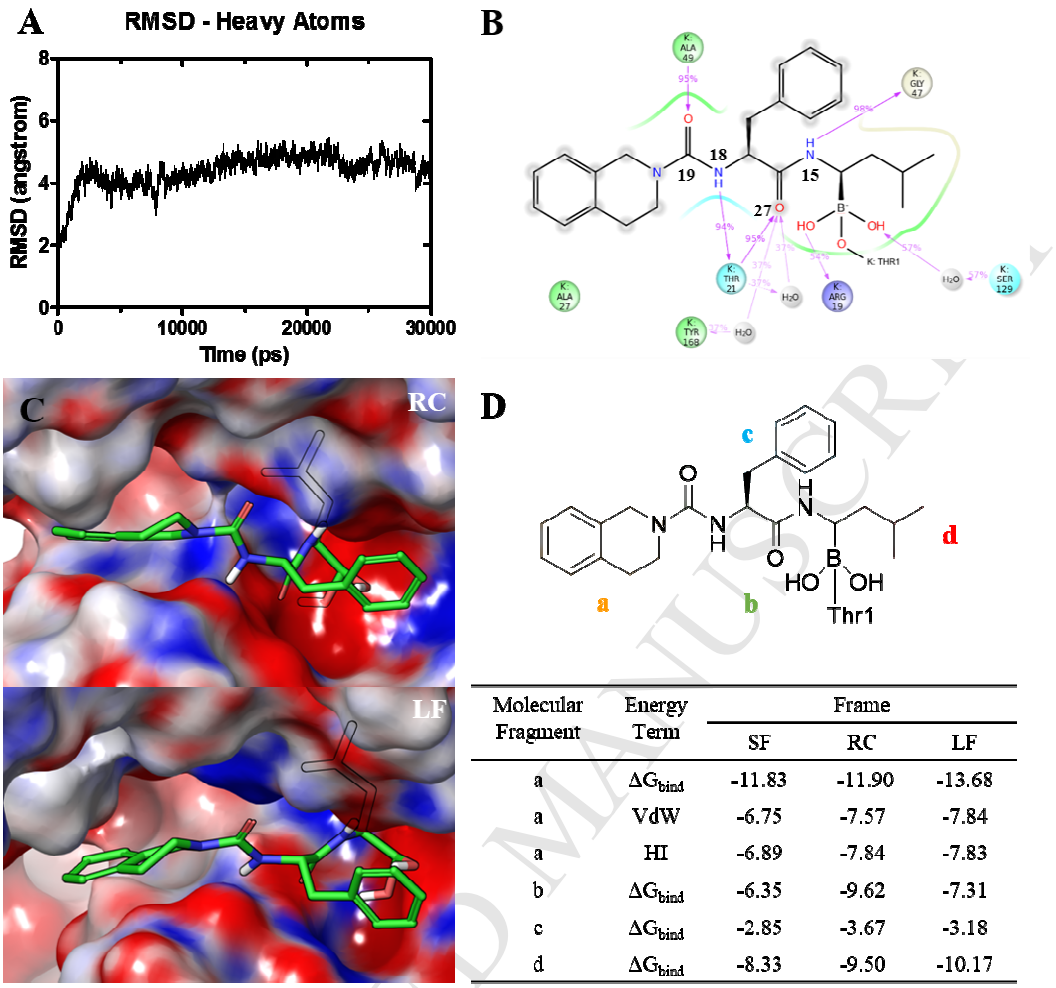

Molecular Fragment	Energy Term	Frame		
		SF	RC	LF
a	ΔG_{bind}	-11.83	-11.90	-13.68
a	VdW	-6.75	-7.57	-7.84
a	HI	-6.89	-7.84	-7.83
b	ΔG_{bind}	-6.35	-9.62	-7.31
c	ΔG_{bind}	-2.85	-3.67	-3.18
d	ΔG_{bind}	-8.33	-9.50	-10.17

Fig. 7. Molecular dynamics profile of **I-14** within the β5 and β6 subunit inhibitor pocket of yeast 20S proteasome. (A) RMSD of all of the heavy atoms of the complex versus time. (B) 2D interaction graph in 10 to 30 ns. Percentage refers to the frequency of valid corresponding hydrogen bondings throughout the simulation. (C) **I-14** (green sticks) in the inhibitor pocket. Above: Representative conformation (RC) during 10 to 30 ns. Below: Last frame (LF) of the simulation. (D) MM-GBSA chart. Fragments of **I-14** (above) are marked in different colors and letters. Energy contributions (kcal/mol) of the corresponding fragment are listed in the chart below. SF: Starting Frame of the simulation. VdW: Van der Waals interaction. HI: Hydrophobic Interaction.

3. Conclusion

Known drawbacks of Bortezomib and its analogues with peptide backbone include their rapid metabolism, tendency to develop resistance, and dose-limiting toxicities. To overcome these problems, we designed and synthesized a series of urea-containing peptide boronic acids as potent proteasome inhibitors. Most of the synthesized compounds exhibited excellent potency in inhibiting proteasome activities and tumor cell growth. Based on two rounds of investigations, three compounds were selected and their cellular activities were evaluated against eleven tumor cell lines. They all enabled inhibition (IC_{50} < 100 nM) of ten out of eleven tested tumor cell lines. The compound **I-14** was also tested for its *in vivo* anti-tumor activity with the Bel7404

ACCEPTED MANUSCRIPT

xenograft nude mice model. The results showed that compared with Bortezomib, **I-14** demonstrated similar *in vivo* efficacy and significantly lower toxicity in rats. Pharmacokinetic profiles suggested that **I-14** is metabolically more stable than Bortezomib as expected originally. The docking and molecular dynamics studies revealed the interaction mode between **I-14** and the 20S proteasome, and the results may inspire the design of more potent proteasome inhibitors. Additional preclinical profiling studies of **I-14** are currently in progress.

4. Experiment

4.1. General information

All commercial reagents were purchased from commercial suppliers and used without further purification. Dry solvents were prepared according to standard procedures. Melting points were taken with an X4 apparatus and were uncorrected. Yields refer to chromatographically pure compounds unless otherwise stated. ^{1}H-NMR spectra were recorded in $CDCl_3$ and DMSO-d_6 at ambient temperature on a Bruker Avance III 400 MHz system. ^{13}C NMR spectra were recorded in DMSO-d_6 at ambient temperature unless otherwise noted, at 100 MHz. Silica gel column chromatography was performed with silica gel 60 N (spherical, neutral, 63-210 μm, or Merck). MS data were obtained with MDSSCIEX QSTAR systems. Compounds are evaluated for >95% purity using HPLC analysis (methanol/water) using a C18 column.

4.2. General procedures for the synthesis of compounds I-1 and II-1

4.2. 1. (S)-Methyl 2-(3-benzylureido)-3-phenylpropanoate (**I-1a**)

To a solution of *N*,*N*'-carbonyldiimidazole (CDI, 1.64 g, 10.1 mmol) in DMF (8 mL) and acetonitrile (40 mL) was added L-phenylalanine methyl ester hydrochloride (2.0 g, 9.3 mmol) in portions. The solution was stirred at room temperature for 2 h. Benzylamine (1 g, 9.3 mmol) was then added, followed by the addition of triethylamine (1.72 mL, 18.6 mmol), and the aggregation system began to become clear. The reaction mixture was stirred at room temperature for 24 h until completion as monitored by TLC, and then concentrated under reduced pressure. The residue was dissolved in ethyl acetate (50 mL) and washed with brine (50 mL×3), dried over anhydrous Na_2SO_4 and concentrated in vacuo. The crude material was recrystallized from ethyl acetate to afford the product **I-1a** as a white solid (1.22 g, 43% yield); mp: 93–95 °C. ^{1}H NMR (400 MHz, $CDCl_3$) δ 7.18 (m, 8H), 7.2 (d, *J* = 4 Hz, 2H), 5.78 (m, 2H), 4.64 (dd, *J* = 14.3, 6.3 Hz, 1H), 4.14 (tt, *J* = 15.2, 7.8 Hz, 2H), 3.52 (s, 3H), 2.88 (ddd, *J* = 38.2, 13.8, 6.3 Hz, 2H). ^{13}C NMR (101 MHz, $CDCl_3$) δ 173.54, 157.91, 139.41, 136.49, 129.34, 128.49, 128.41, 127.28, 127.05, 126.84, 54.23, 52.05, 44.02, 38.54.

4.2. 2. (S)-2-(3-Benzylureido)-3-phenylpropanoic acid (**I-1b**)

I-1a (1.22 g, 3.9 mmol) was dissolved in 10 mL of acetone, and 2 N NaOH aqueous solution was added dropwise at 0 °C until TLC showed methyl ester **I-1a** was saponified completely (approximately 2 h). The reaction solution was acidified to pH

ACCEPTED MANUSCRIPT

2 with 3 N HCl. Upon standing, the precipitate was filtered and washed with water until pH value reached 6–7. **I-1b** (0.9 g, 78%) was obtained and used in next step without further purification.

4.2.3. (S)-2-(3-Benzylureido)-*N*-((R)-3-methyl-1-(4,4,5,5-tetramethyl-1,3,2-dioxaborolan-2-yl)butyl)-3-phenylpropanamide (**I-1c**)

To a stirred suspension of **I-1b** (0.9 g, 3.0 mmol) in CH_2Cl_2 (50 mL) were added dicyclohexylcarbodiimide (DCC, 0.74 g, 3.6 mmol) and 1-hydroxybenzotriazole monohydrate (HOBt, 0.45 g, 3.3 mmol). Pinacol leucine boronate hydrochloride **1** (0.75 g, 3.0 mmol, prepared according to the literature[21]) and DIPEA (0.52 mL, 3.0 mmol) were then added. The mixture was stirred at room temperature for 24 h and then filtered to remove the insoluble material. The solvent was removed under vacuum, and the residue was dissolved in 50 mL of ethyl acetate. The organic layer was successively washed with 10% citric acid, 5% $NaHCO_3$ and brine. The organic phase was dried over anhydrous Na_2SO_4. The solvent was evaporated to give product **I-1c** as a faint yellow foam (1.23 g, crude with impurities) and it was used for next step without further purification.

4.2.4. ((R)-1-((S)-2-(3-Benzylureido)-3-phenylpropanamido)-3-methylbutyl)-boronic acid (**I-1**)

To the solution of **I-1c** obtained above in ethyl acetate (40 mL) was added diethanolamine (0.2 mL, 1.1 equiv) dropwise, and the reaction mixture was stirred at room temperature until completion as monitored by TLC. The resulted precipitate was filtered, washed with ethyl acetate, and then taken up with a mixture of ethyl acetate (20 mL) and water (20 mL). To this suspension was added 4N hydrochloric acid under stirring and it was stirred for an additional 2 h. The organic layer was separated and washed with brine (50 mL×3), and dried over anhydrous Na_2SO_4. The organic solvent was removed under reduced pressure to provide product **I-1** (570 mg, 15% in overall) as a white foam. mp: 133–136 ℃. HPLC indicates a purity of 95.2 area %. ^{1}H NMR (400 MHz, DMSO-$_{d6}$) δ 7.41–7.14 (m, 9H), 7.17–7.02 (m, 2H), 6.51 (s, 1H), 6.35 (dd, *J* = 8.4, 4.6 Hz, 1H), 4.70–4.52 (m, 1H), 4.16 (ddd, *J* = 20.4, 15.4, 5.8 Hz, 2H), 3.00 (dd, *J* = 8.9, 4.1 Hz, 1H), 2.91–2.77 (m, 1H), 2.68 (s, 1H), 1.60 (dd, *J* = 13.0, 6.6 Hz, 1H), 1.32 (ddd, *J* = 26.5, 15.3, 6.7 Hz, 2H), 0.84 (d, *J* = 6.2 Hz, 6H). ^{13}C NMR (101 MHz, DMSO-$_{d6}$) δ 174.88, 157.71, 140.93, 137.53, 129.86, 128.61, 128.50, 127.29, 126.96, 126.80, 43.25, 38.96, 25.57, 23.48, 23.20, 23.02, 21.51. HRMS (ESI) calcd for $C_{23}H_{31}BN_3O_3$: 408.24571 [$(M-H_2O+CH_2+H)^+$], found 408.24429.

4.2.5. (S)-*tert*-Butyl (1-((4-methoxybenzyl)amino)-1-oxo-3-phenylpropan-2-yl) carbamate (**II-1a**)

To a solution of *N*-Boc-L-phenylalanine (2.65 g, 10.0 mmol) in THF (50 mL) was added dicyclohexylcarbodiimide (DCC, 2.47 g, 12.0 mmol) and 1-hydroxybenzotriazole monohydrate (HOBt, 1.48 g, 11.0 mmol). The reaction mixture was allowed to stirred for 30 min before 4-methoxybenzylamine (1.3 mL, 10.0 mmol) was added, followed by the addition of *N*-methylmorpholine (1.32 mL,

ACCEPTED MANUSCRIPT

12.0 mmol). The mixture was stirred for another 24 h, filtered and the solvent was removed under vacuum. The residue was dissolved in 50 mL of ethyl acetate and washed with 10% citric acid, 5% $NaHCO_3$ and brine, then dried over anhydrous Na_2SO_4. The crude product was purified by silica gel chromatography (ethyl acetate: petroleum ether = 1:3) to afford the desired product **II-1a** (2.66 g, 6.9 mmol). mp: 68–71 °C. ^{1}H NMR (400 MHz, $CDCl_3$) δ 7.33–7.11 (m, 5H), 7.00 (d, *J* = 7.1 Hz, 2H), 6.77 (d, *J* = 8.5 Hz, 2H), 6.40 (s, 1H), 5.26 (d, *J* = 6.7 Hz, 1H), 4.40 (d, *J* = 17.7 Hz, 1H), 4.24 (qd, *J* = 14.4, 5.2 Hz, 2H), 3.75 (s, 3H), 3.04 (d, *J* = 6.1 Hz, 2H), 1.36 (s, 9H). ^{13}C NMR (101 MHz, $CDCl_3$) δ 171.15, 158.93, 155.49, 136.81, 129.90, 129.37, 128.99, 128.60, 126.83, 113.95, 80.06, 55.26, 42.88, 38.77, 33.97, 28.27.

4.2.6. (S)-2-Amino-*N*-(4-methoxybenzyl)-3-phenylpropanamide hydrochloride (**II-1b**)

To a stirring solution of **II-1a** (2.66 g, 6.9 mmol) in 10 mL of CH_2Cl_2 was added dropwise a solution of 10 M HCl in EtOH (2 mL, 21 mmol) at 0 °C. The reaction mixture was stirred until the starting material was completely consumed. The formed precipitate was filtered, washed with CH_2Cl_2 and dried in vacuum to give **II-1b** without further purification.

4.2.7. (S)-*N*-(4-Methoxybenzyl)-2-(3-((R)-3-methyl-1-(4,4,5,5-tetramethyl-1,3,2-dioxaborolan-2-yl)butyl)ureido)-3-phenylpropanamide (**II-1c**)

To a stirring solution of *N*,*N*'-carbonyldiimidazole (CDI, 0.54 g, 3.3 mmol) in DMF (6 mL) and acetonitrile (30 mL) was added the pinacol leucine boronate hydrochloride **1** (0.75 g, 3.0 mmol) by portions. The solution was stirred at room temperature for 2 h. Then **II-1b** (0.96 g, 3 mmol) was added, followed by the addition of triethylamine (0.83 mL, 6 mmol). The stirring was continued for another 24 h, and acetonitrile was removed under reduced pressure. The residues was dissolved in ethyl acetate (50 mL) and washed with brine (50 mL×3), dried over Na_2SO_4. The solvent was evaporated to give a grey foam product **II-1c** (1.2 g, crude with impurities) which was used in next step without further purification.

4.2.8. ((R)-1-(3-((S)-1-((4-Methoxybenzyl)amino)-1-oxo-3-phenylpropan-2-yl)ureido)-3-methyl butyl)boronic acid (**II-1**)

The previously obtained **II-1c** was dissolved in 40 mL of ethyl acetate and filtered the possible insoluble impurities. Diethanolamine (0.2 mL, 1.1 equiv) was added dropwise. After a few minutes, a white precipitate formed, and the reaction was allowed to continue until the starting material was completely consumed as monitored by TLC. The precipitate was then filtered, washed with ethyl acetate, and then taken into a flask filled with 20 mL ethyl acetate and 20 mL H_2O. To the suspension was added 4 M HCl (1 mL). After about 2 h as judged by TLC, the organic layer was separated and washed with brine (50 mL×3), dried over Na_2SO_4. The organic solvent was removed under reduced pressure to provide the analytically pure product **II-1** (120 mg, 29% in overall) as a white foam. mp: 128–135 °C. HPLC indicates a purity of 95.8 area %. ^{1}H NMR (400 MHz, DMSO-$_{d6}$) δ 8.36 (s, 1H), 6.82–7.21 (m, 10H),

ACCEPTED MANUSCRIPT

4.34 (s, 1H), 4.17 (ddd, *J* = 29.3, 14.6, 5.2 Hz, 2H), 3.71 (s, 3H), 3.07–2.69 (m, 2H), 1.67–1.42 (m, 1H), 1.37–1.04 (m, 2H), 0.79 (t, *J* = 5.6 Hz, 6H). ^{13}C NMR (101 MHz, DMSO-*d6*) δ 158.65, 137.77, 131.28, 129.79, 128.95, 128.76, 128.53, 128.44, 126.79, 114.07, 55.49, 42.04, 41.99, 38.78, 25.78, 23.69, 23.29. HRMS (ESI) calcd for $C_{24}H_{33}BN_3O_4$: 438.25629 [(M-H_2O+CH_2+H)$^+$], found 438.25483.

4.2.9. ((R)-1-((S)-2-(3-(4-Methoxybenzyl)ureido)-3-phenylpropanamido)-3-methyl-butyl) boronic acid (**I-2**)

Using the same procedure as **I-1,** white foam, 31% yield; mp: 126–128 °C. HPLC indicates a purity of 98.8 area %. ^{1}H NMR (400 MHz, DMSO-*d6*) δ 7.31–7.19 (m, 5H), 7.06 (d, *J* = 8.5 Hz, 2H), 6.83 (d, *J* = 8.6 Hz, 2H), 6.42 (s, 1H), 6.30 (d, *J* = 8.5 Hz, 1H), 4.63 (dd, *J* = 13.7, 7.9 Hz, 1H), 4.20–3.98 (m, 2H), 3.71 (s, 3H), 3.04–2.76 (m, 2H), 2.67 (d, *J* = 2.7 Hz, 1H), 1.59 (dd, *J* = 13.1, 6.5 Hz, 1H), 1.40–1.20 (m, 2H), 0.84 (d, *J* = 4.0 Hz, 6H). ^{13}C NMR (101 MHz, DMSO-*d6*) δ 174.96, 158.53, 157.65, 137.61, 132.78, 129.86, 128.64, 128.50, 126.80, 114.04, 55.46, 42.76, 38.97, 25.59, 23.40, 23.27, 21.49. HRMS (ESI) calcd for $C_{24}H_{33}BN_3O_4$: 438.25629 [(M-H_2O+CH_2+H)$^+$], found 438.25508.

4.2.10. ((R)-1-((S)-2-(3-(3-(Benzyloxy)phenyl)ureido)-3-phenylpropanamido)-3-methyl-butyl)boronic acid (**I-3**)

Using the same procedure as **I-1**, white foam, 26% yield; mp: 112–115 °C. HPLC indicates a purity of 97.5 area %. ^{1}H NMR (400 MHz, DMSO-*d6*) δ 8.84 (d, *J* = 17.7 Hz, 1H), 8.67 (d, *J* = 9.8 Hz, 1H), 7.52–7.16 (m, 11H), 7.10 (dt, *J* = 13.7, 6.8 Hz, 1H), 6.86 (d, *J* = 6.6 Hz, 1H), 6.57 (d, *J* = 8.1 Hz, 1H), 6.45 (dd, *J* = 19.5, 8.9 Hz, 1H), 5.04 (s, 2H), 4.77–4.57 (m, 1H), 3.12–2.87 (m, 2H), 2.72 (s, 1H), 1.59 (dt, *J* = 13.1, 9.2 Hz, 1H), 1.45–1.20 (m, 2H), 0.84 (d, *J* = 5.4 Hz, 6H). ^{13}C NMR (101 MHz, DMSO-*d6*) δ 174.37, 159.25, 154.75, 141.85, 137.64, 137.26, 129.93, 129.87, 128.84, 128.57, 128.18, 128.00, 126.91, 110.77, 108.01, 104.91, 69.52, 52.18 (m), 38.97, 33.84, 25.54, 23.60, 22.94, 21.49. HRMS (ESI) calcd for $C_{29}H_{35}BN_3O_4$: 500.27202 [(M-H_2O+CH_2+H)$^+$], found 500.27025.

4.2.11. ((R)-3-Methyl-1-((S)-3-phenyl-2-(3-(pyrazin-2-yl)ureido)propanamido)butyl) -boronic acid (**I-4**)

Using the same procedure as **I-1**, yellow-white foam, 17% yield; mp: 135–138 °C. HPLC indicates a purity of 97.2 area %. ^{1}H NMR (400 MHz, DMSO-*d6*) δ 9.54 (s, 1H), 8.86 (d, *J* = 14.4 Hz, 1H), 8.76 (d, *J* = 6.0 Hz, 1H), 8.17 (dd, *J* = 9.2, 5.6 Hz, 2H), 7.94 (d, *J* = 6.6 Hz, 1H), 7.22 (dt, *J* = 27.6, 4.1 Hz, 5H), 4.82–4.62 (m, 1H), 3.14–2.90 (m, 2H), 2.64 (br, 1H), 1.56 (dt, *J* = 13.1, 6.6 Hz, 1H), 1.39–1.12 (m, 2H), 0.78 (dd, *J* = 6.1, 2.6 Hz, 6H). ^{13}C NMR (101 MHz, DMSO-*d6*) δ 173.89, 154.06, 150.00, 141.47, 137.59, 136.92, 135.47, 130.00, 128.59, 127.07, 52.47, 38.61, 25.48, 23.49, 23.01, 22.93. HRMS (ESI) calcd for $C_{20}H_{27}BN_5O_3$: 396.22050 [(M-H_2O+CH_2+H)$^+$], found 396.21998.

ACCEPTED MANUSCRIPT

4.2.12. ((R)-1-((S)-2-(3-(2,5-Dimethoxybenzyl)ureido)-3-phenylpropanamido)-3-methyl-butyl)boronic acid (**I-5**)

Using the same procedure as **I-1**, white foam, 28% yield; mp: 156–159 °C. HPLC indicates a purity of 95.2 area %. ^{1}H NMR (400 MHz, DMSO-$_{d6}$) δ 7.23–7.10 (m, 5H), 6.83 (d, *J* = 8.8 Hz, 1H), 6.76–6.68 (m, 2H), 4.30 (dt, *J* = 13.9, 6.2 Hz, 0H), 4.08 (d, *J* = 5.0 Hz, 2H), 3.97 (m, 2H), 3.69 (s, 3H), 3.63 (s, 3H), 3.10–2.83 (m, 2H), 2.81–2.65 (m, 1H), 1.50–1.14 (m, 1H), 0.90–0.58 (dd, 6H). ^{13}C NMR (101 MHz, DMSO-$_{d6}$) δ 171.93, 158.22, 153.46, 151.14, 137.86, 129.56, 129.27, 128.53, 126.73, 114.62, 112.29, 111.83, 56.13, 55.73, 38.45, 25.18, 24.96, 23.55, 23.52, 22.26, 22.02. HRMS (ESI) calcd for $C_{25}H_{35}BN_3O_5$: 468.26687 [(M-H_2O+CH_2+H)$^+$], found 468.26590.

4.2.13. ((R)-1-((S)-2-(3-(2,3-dichlorobenzyl)ureido)-3-phenylpropanamido)-3-methyl-butyl)boronic acid (**I-6**)

Using the same procedure as **I-1**, white foam, 32% yield; mp: 119–122 °C. HPLC indicates a purity of 96.2 area %. ^{1}H NMR (400 MHz, DMSO-$_{d6}$) δ 7.22 (m, 8H), 7.12 (d, *J* = 4.3 Hz, 1H), 6.49 (s, 1H), 6.33 (d, *J* = 8.7 Hz, 1H), 4.58 (d, *J* = 5.9 Hz, 1H), 4.12 (dt, *J* = 15.3, 10.3 Hz, 2H), 2.98 (d, *J* = 12.4 Hz, 1H), 2.90–2.74 (m, 1H), 2.64 (s, 1H), 1.70–1.45 (m, 1H), 1.28 (m, 2H), 0.83 (d, *J* = 5.5 Hz, 6H). ^{13}C NMR (101 MHz, DMSO-$_{d6}$) δ 175.00, 157.69, 140.98, 137.54, 129.89, 129.82, 128.59, 128.50, 128.40 (m, 18H), 127.29, 126.95, 126.79, 43.24, 38.99, 25.54, 23.60, 23.01, 21.50. HRMS (ESI) calcd for $C_{23}H_{29}BCl_2N_3O_3$: 462.25222 [(M-H_2O+CH_2+H)$^+$], found 462.25277.

4.2.14. (R)-(1-(2-(3-(3-(Benzyloxy)phenyl)ureido)acetamido)-3-methylbutyl)boronic acid (**I-7**)

Using the same procedure as **I-1**, white foam, 36% yield; mp: 109–113 °C. HPLC indicates a purity of 95.6 area %. ^{1}H NMR (400 MHz, DMSO-$_{d6}$) δ 8.82 (s, 1H), 8.77 (s, 1H), 7.37 (m, 5H), 7.26 (s, 1H), 7.13 (t, *J* = 8.1 Hz, 1H), 6.92 (d, *J* = 7.8 Hz, 1H), 6.64–6.54 (m, 1H), 6.47 (t, *J* = 5.2 Hz, 1H), 5.05 (s, 2H), 3.92 (d, *J* = 4.6 Hz, 2H), 2.64 (s, 1H), 1.62 (dt, *J* = 13.2, 6.6 Hz, 1H), 1.44–1.20 (m, 2H), 0.83 (d, *J* = 4.9 Hz, 6H). ^{13}C NMR (101 MHz, DMSO-$_{d6}$) δ 173.08, 159.24, 155.44, 142.00, 137.65, 129.87, 128.84, 128.18, 128.00, 110.86, 108.02, 104.97, 69.51, 43.5 (m), 40.85, 25.62, 23.39, 23.25, 21.49. HRMS (ESI) calcd for $C_{22}H_{29}BN_3O_4$: 410.22495 [(M-H_2O+CH_2+H)$^+$], found 410.22377.

4.2.15. (R)-(1-(2-(3-(2,5-Dichlorophenyl)ureido)acetamido)-3-methylbutyl)boronic acid (**I-8**)

Using the same procedure as **I-1**, white foam, 17% yield; mp: 125–129 °C. HPLC indicates a purity of 95.2 area %. ^{1}H NMR (400 MHz, DMSO-$_{d6}$) δ 8.79 (s, 1H), 8.47 (d, *J* = 10.7 Hz, 1H), 8.30 (d, *J* = 2.2 Hz, 1H), 7.57 (dd, *J* = 10.3, 5.3 Hz, 1H), 7.41 (dd, *J* = 8.5, 4.3 Hz, 1H), 7.00 (dd, *J* = 8.5, 2.2 Hz, 1H), 3.95 (d, *J* = 4.8 Hz, 2H), 3.37 (m, 1H), 1.61 (m, 1H), 1.38–1.17 (m, 2H), 0.83 (dd, *J* = 13.9, 3.7 Hz, 6H). ^{13}C NMR (101 MHz, DMSO-$_{d6}$) δ 172.63, 168.84, 155.05, 138.26, 132.30, 130.79, 122.41, 119.91, 43.04, 25.60, 23.34, 23.17, 22.91. HRMS (ESI) calcd for $C_{15}H_{21}BCl_2N_3O_3$:

372.10502 [(M-H_2O+CH_2+H) $^+$], found 372.10413.

4.2.16. ((R)-1-((S)-2-((S)-2-(3-(3-(Benzyloxy)phenyl)ureido)-3-phenylpropanamido)-3-phenylpropanamido)-3-methylbutyl)boronic acid (**I-9**)

Using the same procedure as **I-1**, white foam, 18% yield; mp: 130–133 °C. HPLC indicates a purity of 96.4 area %. ^{1}H NMR (400 MHz, DMSO-$_{d6}$) δ 8.72 (d, *J* = 5.6 Hz, 1H), 8.65 (d, *J* = 16.6 Hz, 1H), 8.55 (s, 1H), 7.48–7.06 (m, 16H), 6.87 (d, *J* = 8.3 Hz, 1H), 6.80 (d, *J* = 4.0 Hz, 1H), 6.64–6.50 (m, 1H), 6.24 (d, *J* = 5.9 Hz, 1H), 5.04 (s, 2H), 4.68 (dd, *J* = 14.3, 6.5 Hz, 1H), 4.51 (dd, *J* = 16.6, 6.0 Hz, 1H), 3.00 (dd, *J* = 35.2, 22.1 Hz, 2H), 2.88–2.64 (m, 2H), 1.59 (s, 1H), 1.31 (dd, *J* = 23.7, 18.0 Hz, 2H), 0.79 (dd, *J* = 21.1, 5.3 Hz, 6H). ^{13}C NMR (101 MHz, DMSO-$_{d6}$) δ 172.42, 171.75, 159.25, 154.96, 141.92 , 137.64, 129.88, 129.84, 129.74, 128.84, 128.83, 128.51, 128.36, 128.18, 127.99, 126.69, 126.60, 110.69, 107.92, 104.87, 69.54, 54.30, 37.81, 25.51, 23.67, 23.41, 22.98, 22.80, 21.49. HRMS (ESI) calcd for $C_{38}H44BN_4O_5$: 647.34057 [(M-H_2O+CH_2+H) $^+$], found 647.33814.

4.2.17. ((R)-3-Methyl-1-((S)-2-(3-((S)-1-oxo-3-phenyl-1-(pyrazin-2-ylamino)propan-2-yl)ureido)-3-phenylpropanamido)butyl)boronic acid (**I-10**)

Using the same procedure as **I-1**, white foam, 14% yield; mp: 170–174 °C. HPLC indicates a purity of 96.5 area %. ^{1}H NMR (400 MHz, DMSO-$_{d6}$) δ 10.89 (s, 1H), 9.31 (s, 1H), 8.40 (s, 1H), 8.37 (s, 1H), 7.47 (s, 1H), 7.31–7.09 (m, 10H), 6.54 (d, *J* = 7.7 Hz, 1H), 6.40 (d, *J* = 7.6 Hz, 1H), 4.67 (d, *J* = 4.3 Hz, 1H), 4.29 (d, *J* = 5.5 Hz, 1H), 3.10–2.94 (m, 2H), 2.79 (ddd, *J* = 21.0, 13.6, 8.0 Hz, 2H), 1.50 (dd, *J* = 12.7, 6.4 Hz, 1H), 1.41–1.10 (m, 2H), 0.78 (dd, *J* = 27.1, 6.5 Hz, 6H). ^{13}C NMR (101 MHz, DMSO-$_{d6}$) δ 172.61, 171.53, 157.53, 149.07, 143.11, 140.24, 138.27, 137.80, 136.69, 129.80, 129.76, 128.55, 128.37, 126.82, 126.47, 55.49, 54.67, 38.77, 38.35, 25.18, 23.71, 23.66, 22.46. HRMS (ESI) calcd for $C_{29}H_{36}BN_6O_4$: 543.28907 [(M-H_2O+CH_2+H) $^+$], found 543.28785.

4.2.18. ((R)-1-(3-((S)-1-((3-(Benzyloxy)phenyl)amino)-1-oxo-3-phenylpropan-2-yl)-ureido)-3-methylbutyl)boronic acid (**II-2**)

Using the same procedure as **II-1**, white foam, 27% yield; mp: 113–115 °C. HPLC indicates a purity of 98.2 area %. ^{1}H NMR (400 MHz, DMSO-$_{d6}$) δ 10.12 (s, 1H), 7.58–7.06 (m, 16H), 6.73 (d, *J* = 7.0 Hz, 1H), 5.07 (s, 2H), 4.53 (s, 1H), 3.03 (s, 1H), 2.90 (s, 1H), 1.64–1.42 (m, 1H), 1.20 (dd, *J* = 14.5, 8.5 Hz, 2H), 0.85–0.68 (s, 6H). ^{13}C NMR (101 MHz, DMSO-$_{d6}$) δ 170.72, 159.07, 140.31, 137.47, 130.00, 129.77, 129.55, 128.89, 128.56, 128.28, 128.09, 126.91, 112.42, 110.07, 106.68, 69.60, 56.19, 41.91, 25.77, 23.67, 23.20, 21.52. HRMS (ESI) calcd for $C_{29}H_{35}BN_3O_4$: 500.27202 [(M-H_2O+CH_2+H) $^+$], found 500.27051.

4.2.19. ((R)-3-Methyl-1-(3-((S)-1-oxo-3-phenyl-1-(pyrazin-2-ylamino)propan-2-yl)-ureido)butyl)boronic acid (**II-3**)

Using the same procedure as **II-1**, white foam, 22% yield; mp: 145–148 °C. HPLC indicates a purity of 97.2 area %. ^{1}H NMR (400 MHz, DMSO-$_{d6}$) δ 10.96 (s, 1H),

ACCEPTED MANUSCRIPT

9.30 (s, 1H), 8.41 (s, 1H), 8.38 (d, *J* = 1.7 Hz, 1H), 7.42–7.17 (m, 5H), 7.17 (d, *J* = 6.4 Hz, 1H), 4.65 (s, 1H), 3.14–2.81 (m, 2H), 2.41 (s, 1H), 1.45 (dd, *J* = 12.7, 6.3 Hz, 1H), 1.32–1.05 (m, 2H), 0.71 (t, *J* = 7.0 Hz, 6H). ^{13}C NMR (101 MHz, DMSO-$_{d6}$) δ 161.07, 148.94, 143.12, 140.40, 137.51, 136.63, 129.80, 128.56, 126.95, 56.03, 41.74, 25.69, 23.56, 23.14, 21.51. HRMS (ESI) calcd for $C_{20}H_{27}BN_5O_3$: 396.22050 [(M-H_2O+CH_2+H)$^+$], found 396.21936.

4.2.20. ((R)-1-(3-((S)-1-((4-Methoxyphenyl)amino)-1-oxo-3-phenylpropan-2-yl)ureido)-3-methylbutyl)boronic acid (**II-4**)

Using the same procedure as **II-1**, white foam, 25% yield; mp: 146–148 °C. HPLC indicates a purity of 96.2 area %. ^{1}H NMR (400 MHz, DMSO-$_{d6}$) δ 9.91 (s, 1H), 7.45 (d, *J* = 8.9 Hz, 2H), 7.20 (m, 5H), 7.18 (d, *J* = 6.0 Hz, 1H), 6.88 (d, *J* = 9.0 Hz, 2H), 4.50 (d, *J* = 5.4 Hz, 1H), 3.71 (s, 3H), 3.13–2.79 (m, 2H), 1.53 (td, *J* = 12.9, 6.3 Hz, 1H), 1.34–1.09 (m, 2H), 0.91–0.70 (t, *J* = 4.0 Hz, 6H). ^{13}C NMR (101 MHz, DMSO-$_{d6}$) δ 172.46, 169.90, 155.90, 137.66, 132.15, 129.78, 128.54, 126.86, 121.50, 114.30, 55.61, 41.95, 38.85, 25.78, 23.69, 23.20. HRMS (ESI) calcd for $C_{23}H_{31}BN_3O_4$: 424.24062 [(M-H_2O+CH_2+H)$^+$], found 424.23945.

4.2.21. ((R)-3-Methyl-1-(3-((R)-1-oxo-3-phenyl-1-(pyrazin-2-ylamino)propan-2-yl) ureido)butyl)boronic acid (**II-5**)

Using the same procedure as **II-1**, white foam, 24% yield; mp: 138–141 °C. HPLC indicates a purity of 95.9 area %. ^{1}H NMR (400 MHz, DMSO-$_{d6}$) δ 11.12–10.93 (m, 1H), 9.45–9.22 (m, 1H), 8.40 (s, 1H), 8.37 (s, 1H), 7.28 (d, *J* = 18.4 Hz, 5H), 7.21–7.15 (m, 1H), 6.52 (s, 1H), 4.68 (s, 1H), 2.92 (dd, *J* = 50.3, 43.2 Hz, 2H), 2.44 (s, 1H), 1.45 (dd, *J* = 12.6, 6.3 Hz, 1H), 1.13 (ddd, *J* = 20.3, 12.1, 6.9 Hz, 3H), 0.77–0.61 (dd, *J* = 6.9, 4.2 Hz, 6H). ^{13}C NMR (101 MHz, DMSO-$_{d6}$) δ 172.45, 160.69, 148.96, 143.11, 140.39, 137.52, 136.66, 129.83, 128.53, 126.92, 55.88, 41.92, 25.66, 23.61, 23.57, 23.06, 21.49. HRMS (ESI) calcd for $C_{20}H_{27}BN_5O_3$: 396.22050 [(M-H_2O+CH_2+H)$^+$], found 396.21952.

4.2.22. ((R)-3-Methyl-1-(3-((S)-4-methyl-1-(((S)-4-methyl-1-oxo-1-(pyrazin-2-ylamino)pentan-2-yl)amino)-1-oxopentan-2-yl)ureido)butyl)boronic acid (**II-6**)

Using the same procedure as **II-1**, white foam, 21% yield; mp: 157–162 °C. HPLC indicates a purity of 95.1 area %. ^{1}H NMR (400 MHz, DMSO-$_{d6}$) δ 10.95 (s, 1H), 9.29 (s, 1H), 8.40 (s, 1H), 8.36 (d, *J* = 2.3 Hz, 1H), 8.13 (d, *J* = 7.2 Hz, 1H), 6.67 (s, 1H), 4.63 (s, 1H), 4.20 (dd, *J* = 15.8, 12.3 Hz, 1H), 1.77–1.10 (m, 9H), 0.99–0.73 (m, 18H). ^{13}C NMR (101 MHz, DMSO-$_{d6}$) δ 173.57, 172.60, 149.09, 143.10, 140.31, 140.27, 136.80, 52.37, 52.02, 42.10, 41.07, 25.69, 24.66, 24.49, 23.71, 23.58, 23.30, 22.36, 21.89, 21.83. HRMS (ESI) calcd for $C_{23}H_{40}BN_6O_4$: 475.32027 [(M-H_2O+CH_2+H)$^+$], found 475.31908.

4.2.23. ((R)-3-Methyl-1-(3-((S)-1-(((S)-4-methyl-1-oxo-1-(pyrazin-2-ylamino)pentan-2-yl) amino)-1-oxo-3-phenylpropan-2-yl)ureido)butyl)boronic acid (**II-7**)

ACCEPTED MANUSCRIPT

Using the same procedure as **II-1**, white foam, 38% yield; mp: 154–157 °C. HPLC indicates a purity of 98.7 area %. ^{1}H NMR (400 MHz, DMSO-$_{d6}$) δ 10.93 (s, 1H), 9.33 (s, 1H), 8.42 (d, *J* = 1.4 Hz, 1H), 8.39 (d, *J* = 2.4 Hz, 1H), 8.24 (dd, *J* = 18.5, 7.8 Hz, 1H), 7.31–6.97 (m, 5H), 4.66 (dd, *J* = 13.8, 7.5 Hz, 1H), 4.50–4.26 (m, 1H), 3.14–2.69 (m, 2H), 1.75–1.47 (m, 4H), 1.39–1.11 (m, 2H), 0.89 (dd, *J* = 11.9, 6.4 Hz, 6H), 0.80 (t, *J* = 5.6 Hz, 6H). ^{13}C NMR (101 MHz, DMSO-$_{d6}$) δ 172.45, 172.43, 149.08, 143.11, 140.35, 137.68, 136.86, 129.83, 129.51, 128.34, 126.65, 52.03, 42.04, 41.12, 25.71, 24.66, 23.73, 23.52, 23.24, 22.02, 21.49. HRMS (ESI) calcd for $C_{26}H_{38}BN6O_4$: 509.30467 [(M-H_2O+CH_2+H)$^+$], found 509.30313.

4.2.24. ((R)-3-Methyl-1-((S)-2-(3-phenethylureido)-3-phenylpropanamido)butyl) boronic acid (**I-11**)

Using the same procedure as **I-1**, white foam, 18% yield; mp: 134–137 °C. HPLC indicates a purity of 96.6 area %. ^{1}H NMR (400 MHz, DMSO-$_{d6}$) δ 8.63 (d, *J* = 17.7 Hz, 1H), 7.33–7.06 (m, 10H), 6.37–6.24 (m, 1H), 6.05 (s, 1H), 4.55 (dd, *J* = 16.1, 8.1 Hz, 1H), 3.26–3.09 (m, 2H), 2.87 (ddd, *J* = 21.9, 13.6, 7.1 Hz, 2H), 2.61 (m, 3H), 1.75–1.44 (m, 1H), 1.45–1.13 (m, 2H), 0.82 (d, *J* = 5.9 Hz, 6H). ^{13}C NMR (101 MHz, DMSO-$_{d6}$) δ 174.98, 157.58, 140.06, 137.66, 129.83, 129.08, 128.73, 128.49, 126.79, 126.42, 52.62, 41.39, 38.95, 36.47, 25.53, 23.40, 23.26. HRMS (ESI) calcd for $C_{24}H_{33}BN_3O_3$: 422.26137 [(M-H_2O+CH_2+H)$^+$], found 422.26053.

4.2.25. ((R)-3-Methyl-1-((S)-3-phenyl-2-(3-((R)-1-phenylethyl)ureido)propanamido)-butyl)boronic acid (**I-12**)

Using the same procedure as **I-1**, white foam, 23% yield; mp: 151–154 °C. HPLC indicates a purity of 95.2 area %. ^{1}H NMR (400 MHz, DMSO-$_{d6}$) δ 8.61 (s, 1H), 7.38–7.07 (m, 10H), 6.53 (d, *J* = 7.9 Hz, 1H), 6.12 (d, *J* = 8.5 Hz, 1H), 4.69 (p, *J* = 6.8 Hz, 1H), 4.52 (dd, *J* = 14.4, 7.5 Hz, 1H), 2.89 (ddd, *J* = 21.2, 13.6, 6.8 Hz, 2H), 2.63 (s, 1H), 1.53 (dt, *J* = 13.1, 6.5 Hz, 1H), 1.34–1.15 (m, 2H), 1.27 (d, *J* = 4.8 Hz, 3H), 0.79 (t, *J* = 6.2 Hz, 6H). ^{13}C NMR (101 MHz, DMSO-$_{d6}$) δ 174.69, 156.86, 145.73, 137.49, 129.91, 128.60, 128.48, 126.87, 126.78, 126.22, 52.49, 49.07, 39.09, 25.46, 23.74, 23.66, 22.86. HRMS (ESI) calcd for $C_{24}H_{33}BN_3O_3$: 422.26137 [(M-H_2O+CH_2+H)$^+$], found 422.26043.

4.2.26. ((R)-3-Methyl-1-((S)-3-phenyl-2-(3-((S)-1-phenylethyl)ureido)propanamido) butyl)boronic acid (**I-13**)

Using the same procedure as **I-1**, white foam, 32% yield; mp: 164–167 °C. HPLC indicates a purity of 95.2 area %. ^{1}H NMR (400 MHz, DMSO-$_{d6}$) δ 8.58 (s, 1H), 7.31–7.17 (m, 10H), 6.51 (d, *J* = 7.8 Hz, 1H), 6.15 (d, *J* = 8.7 Hz, 1H), 4.72–4.62 (m, 1H), 4.53 (dd, *J* = 14.3, 8.0 Hz, 1H), 3.01–2.74 (m, 2H), 2.62 (d, *J* = 3.4 Hz, 1H), 1.54 (dt, *J* = 13.2, 6.6 Hz, 1H), 1.30–1.17 (m, 2H), 1.25 (d, *J* = 5.3 Hz, 3H), 0.79 (d, *J* = 6.6 Hz, 6H). ^{13}C NMR (101 MHz, DMSO-$_{d6}$) δ 174.77, 156.92, 145.62, 137.51,

ACCEPTED MANUSCRIPT

129.86, 128.64, 128.49, 126.90, 126.82, 126.25, 52.64, 49.10, 39.07, 25.54, 23.76, 23.37, 23.24. HRMS (ESI) calcd for $C_{24}H_{33}BN_3O_3$: 422.26137 [$(M-H_2O+CH_2+H)^+$], found 422.26051.

4.2.27. ((R)-3-Methyl-1-((S)-3-phenyl-2-(1,2,3,4-tetrahydroisoquinoline-2-carboxamido)propanamido)butyl)boronic acid (**I-14**)

Using the same procedure as **I-1**, white foam, 28% yield; mp: 158–160 °C. HPLC indicates a purity of 97.0 area %. ^{1}H NMR (400 MHz, DMSO-$_{d6}$) δ 8.64 (s, 1H), 7.39–6.93 (m, 9H), 6.76 (d, *J* = 8.2 Hz, 1H), 4.57 (dd, *J* = 14.2, 8.7 Hz, 1H), 4.52–4.36 (m, 2H), 3.50 (t, *J* = 5.7 Hz, 2H), 3.01 (ddd, *J* = 22.8, 13.4, 7.4 Hz, 2H), 2.66 (d, *J* = 5.5 Hz, 2H), 1.58 (td, *J* = 13.2, 6.6 Hz, 1H), 1.38–1.16 (m, 2H), 0.81 (dd, *J* = 6.5, 2.7 Hz, 6H). ^{13}C NMR (101 MHz, DMSO-$_{d6}$) δ 175.25, 172.44, 157.02, 138.32, 135.20, 134.39, 129.80, 128.90, 128.42, 126.60, 126.53, 126.38, 53.97, 45.73, 41.50, 37.81, 28.61, 25.58, 23.47, 23.15, 21.50. HRMS (ESI) calcd for $C_{25}H_{33}BN_3O_3$: 434.26139 [$(M-H_2O+CH_2+H)^+$], found 434.26060.

4.2.28. ((R)-1-((S)-2-(3-Benzyl-3-methylureido)-3-phenylpropanamido)-3-methylbutyl)-boronic acid (**I-15**)

Using the same procedure as **I-1**, white foam, 31% yield; mp: 111–114 °C. HPLC indicates a purity of 95.3 area %. ^{1}H NMR (400 MHz, DMSO-$_{d6}$) δ 8.71 (s, 1H), 7.31–7.18 (m, 8H), 6.99 (d, *J* = 6.9 Hz, 2H), 6.60 (d, *J* = 8.4 Hz, 1H), 4.66 (td, *J* = 9.1, 5.2 Hz, 1H), 4.36 (dd, *J* = 75.5, 15.8 Hz, 2H), 3.04 (ddd, *J* = 23.6, 13.6, 7.5 Hz, 2H), 2.70 (s, 3H), 1.65 (td, *J* = 13.3, 6.7 Hz, 1H), 1.46–1.20 (m, 2H), 0.87 (d, *J* = 6.5 Hz, 6H). ^{13}C NMR (101 MHz, DMSO-$_{d6}$) δ 175.43, 157.65, 138.85, 138.34, 129.80, 128.73, 128.49, 127.51, 127.17, 126.68, 53.92, 51.53, 37.80, 34.13, 25.66, 23.54, 23.29. HRMS (ESI) calcd for $C_{24}H_{33}BN_3O_3$: 422.26137 [$(M-H_2O+CH_2+H)^+$], found 422.26058.

4.2.29. ((R)-1-((S)-2-(3-(2,3-Dimethylbenzyl)ureido)-3-phenylpropanamido)-3-methylbutyl)boronic acid (**I-16**)

Using the same procedure as **I-1**, white foam, 19% yield; mp: 137–139 °C. HPLC indicates a purity of 98.3 area %. ^{1}H NMR (400 MHz, DMSO-$_{d6}$) δ 7.24 (s, 5H), 7.07–6.89 (m, 3H), 6.33 (s, 1H), 6.27 (d, *J* = 8.2 Hz, 1H), 4.71–4.52 (m, 1H), 4.13 (ddd, *J* = 26.3, 18.5, 6.4 Hz, 2H), 3.07–2.77 (m, 2H), 2.67 (s, 1H), 2.21 (s, 3H), 2.07 (s, 3H), 1.60 (td, *J* = 13.2, 6.6 Hz, 1H), 1.30 (ddd, *J* = 21.8, 12.4, 6.2 Hz, 2H), 0.84 (d, *J* = 5.9 Hz, 6H). ^{13}C NMR (101 MHz, DMSO-$_{d6}$) δ 174.86, 157.46, 138.14, 137.51, 136.58, 134.39, 129.89, 129.84, 128.78, 128.49, 126.79, 125.84, 125.56, 52.64, 42.11, 38.99, 25.57, 23.61, 23.47, 23.01, 20.46, 14.67. HRMS (ESI) calcd for $C_{25}H_{35}BN_3O_3$: 436.27704 [$(M-H_2O+CH_2+H)^+$], found 436.27918.

4.2.30. ((R)-3-Methyl-1-((S)-3-phenyl-2-(3-(pyrazin-2-ylmethyl)ureido)propanamido) butyl)boronic acid (**I-17**)

ACCEPTED MANUSCRIPT

Using the same procedure as **I-1**, white foam, 18% yield; mp: 154–157 °C. HPLC indicates a purity of 97.0 area %. ^{1}H NMR (400 MHz, DMSO-$_{d6}$) δ 8.53 (d, *J* = 1.2 Hz, 1H), 8.49 (d, *J* = 2.5 Hz, 1H), 8.43 (s, 1H), 7.35–7.08 (m, 5H), 6.71 (d, *J* = 5.7 Hz, 1H), 6.58 (dd, *J* = 13.4, 5.1 Hz, 1H), 4.70–4.50 (m, 1H), 4.31 (qd, *J* = 16.6, 5.7 Hz, 2H), 2.90 (ddd, *J* = 22.2, 13.4, 6.6 Hz, 2H), 2.66 (d, *J* = 2.9 Hz, 1H), 1.57 (dd, *J* = 13.3, 6.6 Hz, 1H), 1.41–1.16 (m, 2H), 0.82 (d, *J* = 6.4 Hz, 6H). ^{13}C NMR (101 MHz, DMSO-$_{d6}$) δ 172.46, 157.67, 155.48, 144.08, 143.50, 143.34, 137.59, 129.81, 128.47, 126.82, 52.74, 43.44, 38.86, 25.58, 23.38, 23.24, 21.49. HRMS (ESI) calcd for $C_{21}H_{29}BN_5O_3$: 410.23617 [(M-H_2O+CH_2+H)$^+$], found 410.23521.

4.2.31. ((R)-1-((S)-2-(3-(2,5-Dichlorobenzyl)ureido)-3-phenylpropanamido)-3-methylbutyl)boronic acid (**I-18**)

Using the same procedure as **I-1**, white foam, 18% yield; mp: 118–120 °C. HPLC indicates a purity of 96.2 area %. ^{1}H NMR (400 MHz, DMSO-$_{d6}$) δ 7.41 (m, 1H), 7.23 (m, 7H), 6.65 (d, *J* = 3.2 Hz, 1H), 6.53 (dd, *J* = 10.2, 5.7 Hz, 1H), 4.59 (dd, *J* = 13.7, 6.7 Hz, 1H), 4.26 (d, *J* = 5.9 Hz, 1H), 4.16 (d, *J* = 15.6 Hz, 3H), 3.01 (d, *J* = 11.9 Hz, 1H), 2.88 (d, *J* = 9.3 Hz, 1H), 2.69 (s, 1H), 1.59 (dt, *J* = 17.1, 6.5 Hz, 1H), 1.40–1.22 (m, 2H), 0.84 (d, *J* = 6.2 Hz, 6H).^{13}C NMR (101 MHz, DMSO-$_{d6}$) δ 174.25, 157.85, 140.58, 137.94, 132.34, 131.09, 130.80, 129.69, 128.61, 128.50, 126.88, 54.41, 41.02, 37.88, 25.56, 23.52, 23.45, 23.10, 23.00. HRMS (ESI) calcd for $C_{23}H_{29}BCl_2N_3O_3$: 476.16776 [(M-H_2O+CH_2+H)$^+$], found 476.16698.

4.2.32. ((R)-1-((S)-2-(3-([1,1'-Biphenyl]-4-ylmethyl)ureido)-3-phenylpropanamido)-3-methylbutyl)boronic acid (**I-19**)

Using the same procedure as **I-1**, white foam, 19% yield; mp: 164–167 °C. HPLC indicates a purity of 98.0 area %. ^{1}H NMR (400 MHz, DMSO-$_{d6}$) δ 7.63 (d, *J* = 8.3 Hz, 2H), 7.56 (d, *J* = 7.1 Hz, 2H), 7.45 (t, *J* = 7.5 Hz, 2H), 7.35 (t, *J* = 7.3 Hz, 1H), 7.31–7.19 (m, 7H), 6.59 (s, 1H), 6.48–6.32 (m, 1H), 4.66 (dd, *J* = 14.4, 7.0 Hz, 1H), 4.23 (ddd, *J* = 20.6, 15.6, 5.8 Hz, 2H), 3.14–2.82 (m, 2H), 2.73 (t, *J* = 16.0 Hz, 1H), 1.71–1.55 (m, 1H), 1.34 (ddd, *J* = 24.5, 12.7, 6.3 Hz, 2H), 0.86 (d, *J* = 6.0 Hz, 6H). ^{13}C NMR (101 MHz, DMSO-$_{d6}$) δ 172.45, 157.72, 140.54, 140.23, 139.01, 137.54, 129.94, 129.89, 129.34, 128.53, 127.94, 127.70, 127.00, 126.96, 52.52, 43.04, 39.02, 25.61, 23.62, 23.05, 21.50. HRMS (ESI) calcd for $C_{29}H_{35}BN_3O_3$: 484.27710 [(M-H_2O+CH_2+H)$^+$], found 484.27583.

4.2.33. ((R)-1-((S)-2-(3-(Furan-2-ylmethyl)ureido)-3-phenylpropanamido)-3-methylbutyl) boronic acid (**I-20**)

Using the same procedure as **I-1**, white foam, 30% yield; mp: 120–124 °C. HPLC indicates a purity of 97.9 area %. ^{1}H NMR (400 MHz, DMSO-$_{d6}$) δ 8.67 (s, 1H), 7.53 (d, *J* = 0.9 Hz, 1H), 7.32–7.18 (m, 5H), 6.52–6.25 (m, 3H), 6.10 (d, *J* = 2.7 Hz, 1H), 4.58 (dd, *J* = 14.0, 7.9 Hz, 1H), 4.13 (qd, *J* = 15.7, 5.7 Hz, 2H), 3.04–2.75 (m, 2H), 2.64 (d, *J* = 3.3 Hz, 1H), 1.57 (dt, *J* = 13.2, 6.6 Hz, 1H), 1.37–1.28 (m, 1H), 1.26–1.17

ACCEPTED MANUSCRIPT

(m, 1H), 0.82 (dd, *J* = 6.4, 3.2 Hz, 7H). ^{13}C NMR (101 MHz, DMSO-$_{d6}$) δ 174.82, 157.35, 153.71, 142.28, 137.51, 129.84, 128.50, 126.82, 110.81, 106.64, 52.64, 38.94, 36.85, 25.56, 23.38, 23.24. HRMS (ESI) calcd for $C_{21}H_{29}BN_3O_4$: 398.22494 [(M-H_2O+CH_2+H)$^+$], found 398.22437.

4.2.34. ((R)-3-Methyl-1-((S)-2-(3-(naphthalen-1-ylmethyl)ureido)-3-phenylpropanamido)butyl)boronic acid (**I-21**)

Using the same procedure as **I-1**, white foam, 32% yield; mp: 171–174 °C. HPLC indicates a purity of 95.8 area %. ^{1}H NMR (400 MHz, DMSO-$_{d6}$) δ 8.12–7.98 (m, 1H), 7.93 (dd, *J* = 6.5, 2.8 Hz, 1H), 7.81 (d, *J* = 8.2 Hz, 1H), 7.63–7.50 (m, 2H), 7.50–7.37 (m, 1H), 7.36–7.28 (m, 1H), 7.29–7.18 (m, 5H), 6.59 (d, *J* = 3.0 Hz, 1H), 6.50–6.30 (m, 1H), 4.70 (dd, *J* = 15.4, 6.0 Hz, 2H), 4.57 (dd, *J* = 15.1, 5.3 Hz, 1H), 2.93 (ddd, *J* = 27.6, 13.7, 7.1 Hz, 2H), 2.71 (s, 1H), 1.61 (dd, *J* = 13.3, 6.6 Hz, 1H), 1.50–1.23 (m, 2H), 0.86 (d, *J* = 6.3 Hz, 6H). ^{13}C NMR (101 MHz, DMSO-$_{d6}$) δ 174.94, 157.59, 137.63, 136.04, 133.73, 131.26, 129.87, 128.91, 128.51, 127.74, 126.81, 126.57, 126.15, 125.87, 125.21, 123.82, 52.70, 41.34, 38.99, 25.61, 23.49, 23.23. HRMS (ESI) calcd for $C_{27}H_{33}BN_3O_3$: 458.26142 [(M-H_2O+CH_2+H)$^+$], found 458.26050.

4.2.35. ((R)-1-((S)-2-(3-(3,4-Difluorobenzyl)ureido)-3-phenylpropanamido)-3-methylbutyl) boronic acid (**I-22**)

Using the same procedure as **I-1**, white foam, 35% yield; mp: 163–166 °C. HPLC indicates a purity of 95.4 area %. ^{1}H NMR (400 MHz, DMSO-$_{d6}$) δ 7.67–7.43 (m, 1H), 7.30–7.17 (m, 6H), 7.13 (ddd, *J* = 6.9, 6.2, 2.5 Hz, 1H), 6.93 (d, *J* = 7.9 Hz, 1H), 6.67–6.56 (m, 1H), 6.50–6.36 (m, 1H), 4.57 (dd, *J* = 14.0, 8.1 Hz, 1H), 4.23–4.01 (m, 2H), 3.07–2.75 (m, 2H), 2.65 (d, *J* = 6.7 Hz, 1H), 1.67–1.48 (m, 1H), 1.35–1.23 (m, 2H), 0.82 (d, *J* = 5.9 Hz, 6H). ^{13}C NMR (101 MHz, DMSO-$_{d6}$) δ 174.84, 157.61, 150.30 (dd, *J* = 12.7 Hz, 107.18 Hz), 147.93 (d, *J* = 12.7 Hz, 105.52 Hz), 139.08, 137.55, 129.85, 128.47, 126.80, 123.73, 117.43 (d, *J* = 16.9 Hz), 116.07 (d, *J* = 17.0 Hz), 52.53, 42.24, 38.84, 32.76, 25.53, 23.57, 23.53, 22.96. HRMS (ESI) calcd for $C_{23}H_{29}BF_2N_3O_3$: 444.22549 [(M-H_2O+CH_2+H)$^+$], found 444.22596.

4.2.36. ((R)-3-Methyl-1-((S)-2-(3-(3-nitrobenzyl)ureido)-3-phenylpropanamido)butyl) boronic acid (**I-23**)

Using the same procedure as **I-1**, white foam, 28% yield; mp: 146–149 °C. HPLC indicates a purity of 97.8 area %. ^{1}H NMR (400 MHz, DMSO-$_{d6}$) δ 8.12–7.96 (m, 2H), 7.55 (dt, *J* = 5.2, 2.8 Hz, 2H), 7.36–7.10 (m, 5H), 6.72 (s, 1H), 6.47 (dd, *J* = 16.3, 8.6 Hz, 1H), 4.60 (dd, *J* = 14.2, 7.9 Hz, 1H), 4.43–4.11 (m, 2H), 3.14–2.79 (m, 2H), 2.67 (d, *J* = 6.3 Hz, 1H), 1.58 (dd, *J* = 13.6, 6.8 Hz, 1H), 1.43–1.21 (m, 2H), 0.83 (d, *J* = 4.8 Hz, 6H). ^{13}C NMR (101 MHz, DMSO-$_{d6}$) δ 174.77, 157.66, 148.20, 143.77, 137.49, 134.01, 130.04, 129.87, 128.46, 126.76, 121.90, 121.82, 52.55, 42.65, 38.86, 25.55, 23.55, 22.97. HRMS (ESI) calcd for $C_{23}H_{30}BN_4O_5$: 453.23078 [(M-H_2O+CH_2+H)$^+$], found 453.22971.

ACCEPTED MANUSCRIPT

4.2.37. (S)-Methyl-2-(1-oxo-1,2,3,4-tetrahydroisoquinoline-2-carboxamido)-3-phenylpropanoate (**I-24a**)

Obtained by the oxidation of **I-14a** unexpectedly in the air, yield > 99%; mp: 144–147 °C. ^{1}H NMR (400 MHz, $CDCl_3$) δ 9.98 (d, *J* = 7.0 Hz, 1H), 8.11 (d, *J* = 7.8 Hz, 1H), 7.51 (td, *J* = 7.5, 1.3 Hz, 1H), 7.32 (m, 7H), 4.83 (td, *J* = 7.4, 5.7 Hz, 1H), 4.22–4.07 (m, 2H), 3.75 (s, 3H), 3.19 (ddd, *J* = 21.5, 13.8, 6.6 Hz, 2H), 2.98 (t, *J* = 6.4 Hz, 2H). ^{13}C NMR (101 MHz, $CDCl_3$) δ 172.00, 167.31, 154.65, 139.84, 136.28, 133.28, 129.32, 129.25, 129.05, 128.59, 127.32, 127.07, 127.06, 55.37, 52.28, 41.70, 38.22, 27.87.

4.2.38. ((R)-3-Methyl-1-((S)-2-(1-oxo-1,2,3,4-tetrahydroisoquinoline-2-carboxamido) -3-phenylpropanamido)butyl)boronic acid (**I-24**)

Using the same procedure as **I-1**, white foam, 21% yield; mp: 182–184 °C. HPLC indicates a purity of 96.8 area %. ^{1}H NMR (400 MHz, DMSO-$_{d6}$) δ 8.95 (s, 1H), 8.04 (s, 1H), 7.46 (d, *J* = 7.5 Hz, 1H), 7.39–7.09 (m, 7H), 6.83 (t, *J* = 6.5 Hz, 1H), 4.21 (d, *J* = 5.5 Hz, 1H), 3.52–3.38 (m, 2H), 2.95–2.72 (m, 4H), 1.77 (dd, *J* = 12.9, 6.8 Hz, 1H), 1.47 (ddd, *J* = 20.9, 13.0, 6.3 Hz, 2H), 0.89 (t, *J* = 5.7 Hz, 6H). ^{13}C NMR (101 MHz, DMSO-$_{d6}$) δ 173.57, 171.24, 156.69, 138.09, 136.00, 132.04, 131.12, 130.96, 130.11, 128.55, 127.13, 126.79, 57.41, 50.95, 38.93, 37.15, 25.84, 23.56, 23.24, 21.58. HRMS (ESI) calcd for $C_{24}H_{31}BN_3O_4$: 448.24065 [(M-H_2O+CH_2+H) $^{+}$], found 448.23982.

4.3. Preliminary biological assay

The enzymatic activities of the proteasome were assayed using The Proteasome-Glo™ Cell-Based Assays kit (Promega, USA). The Proteasome-Glo™ Cell-Based Reagents each contain a specific luminogenic proteasome substrate in a buffer optimized for cell permeabilization, proteasome activity and luciferase activity. These peptide substrates are Suc-LLVYaminoluciferin (Succinyl-leucine-leucine-valine-tyrosine-aminoluciferin), Z-LRRaminoluciferin (Z-leucine-arginine-arginine-aminoluciferin) and Z-nLPnLDaminoluciferin (Z-norleucine-proline-norleucine-aspartate-aminoluciferin) for the chymotrypsin-like, trypsin-like and caspase-like activities, respectively. The trypsin-like assay also contains two inhibitors to reduce nonspecific protease activities. Briefly, acute human myeloid leukemic cell line (HL60, 5000 cells/well) were plated 20 μL/well in a 384-well plate. Cells were then equilibrated at 37 °C and 5% CO_2 for 2 h. Serial dilutions of compounds were prepared in culture medium, and 5 μL of each dilution was added to wells. The cells were incubated with the drug at 37 °C and 5% CO_2 for 2 h before 25 μL/well of each Proteasome-Glo™ Cell-Based Reagent was added. The relative luminescence units (RLU) were measured using the Multimode Microplate Reader Varioskan Flash (Thermo Scientific, USA) after 15 min and compared with the RLU of solvent control, and an inhibition rate was calculated.

4.3.1. Biological test of second-round compounds

ACCEPTED MANUSCRIPT

For the enzymatic activities of the proteasome, the same method was used as in the preliminary biological assays, except that IC_{50} was calculated from the curves generated by plotting the percentage of the solvent control versus the test concentration on a logarithmic scale using the SigmaPlot 10.0 software. For the cell growth inhibitory tests, MGC-803, HepG-2 and a standard MTT assay was used to measure cell growth. In brief, a suspension of 3000 cells in 150 μL of medium was added to each well of 96-well plate and allowed to grow. After 24 h, drugs prepared in medium at 10 different concentrations were added to the corresponding plate at a volume of 50 μL per well, and the plate was incubated for 72 h with drugs. Then to each well was added a 20 μL solution of 5 mg/mL MTT and incubation was continued for another 4 h at 37 ℃. Plate was then centrifuged at 1000 rpm at 4 ℃ for 5 min, and the medium was carefully discarded. The formazan crystals were dissolved in 100 μL of DMSO and the absorbance was read using an Infinite M200 (Tecan, Austria) microplate reader at 540 nm.

4.3.2. Anti-tumor spectrum test

We selected three promising compounds (**I-6**, **I-14** and **I-22**) to investigate their inhibitory capacity against 11 human tumor cell lines. The biological assays used the same procedures as mentioned above, and all results were based on three experiments.

4.3.3. In vivo anticancer activity of I-14

Six-week-old male BALB/c athymic nude mice with body weight of 18–20 g (purchased from Shanghai Silaike Animal Co.) were used. Bel7404 tumor blocks were cut into uniform size pieces (about 2 mm) under sterile conditions and subcutaneously implanted into each animal. After the xenograft tumors had grown to a size of ~100 mm^3 (12 days later), mice (n = 6 per group) were given **I-14** (1 mg/kg), Bortezomib (0.5 mg/kg) and control saline (25 mL/kg) every other day for 24 days by intravenous administration via the lateral tail vein. Tumor volumes (calculated using the following formula, $(width)^2 \times length/2$) and body weights were measured 2–3 times a week during the experiment. At the end of the experiment (at day 25), all mice were sacrificed and tumors were isolated and weighed.

4.3.4. Pharmacokinetics study of I-14

A clear aqueous solution of 3 mg/mL **I-14** in 5% DMA + 25% PEG400 + 70% (2% citric acid + 10% HPBCD) was prepared. Three adult male Sprague–Dawley rats (Beijing Vital River Laboratory Animal Technology Co., Ltd.) were used in each treatment group. The solution of **I-14** was administered intravenously at 1 mL/kg via the lateral tail vein as mentioned before. For blood collection, each rat was placed in a clear Plexiglas restraining tube, and blood samples were drawn from the lateral tail vein into heparinized collection tubes at predetermined sampling times (2 min, 5 min, 15 min, 30 min, 1 h, 2 h, 4 h, 8 h, 24 h post dose). At 24 h post dose, the rats were sacrificed by decapitation and trunk blood was obtained. The blood samples were temporarily put on ice until centrifuged to separate the plasma, which were then stored at −20℃ for the initial 24 h and at −80 ℃ afterwards. All experiments and

ACCEPTED MANUSCRIPT

handling of the compound and samples were carried out under protection from light. LC/MS/MS analysis of **I-14** was performed under optimized conditions to obtain the best sensitivity and selectivity of the analyte in selected reaction monitoring mode (SRM). Selected product ions of **I-14** were monitored for quantification using **I-14** (50 ng/mL) in 1:1 v/v methanol/acetonitrile as an internal standard. Plasma concentration–time data were analyzed by a non-compartmental approach using the software WinNonlin Enterprise ver. 4.1 (Pharsight Co., Mountain View, CA).

4.4. Molecular docking

Protein Preparation: Protein structure was downloaded from the RCSB Protein Data Bank (PDB ID: 2F16). All hetero atoms, hydrogen atoms, alternative conformers of residues and the crystal cell were removed. Ligand Preparation: the 3D coordinates of **I-14** and **PS-341** were prepared using Maestro 9.4. Then the initial coordinates were further optimized via the LigPrep module with OPLS_2005 forcefield applied to give the energy-minimized conformation. The boron–oxygen bond length was modified to 1.350 Å to stay in accordance with the crystallized bioactive conformation of **PS-341**. Covalent Docking: The covalent docking was performed via Gold 5.2.2. The center of the cavity was set on protein atom No. 6. With an active site radius of 10.0 Å, the default genetic algorithm (GA) setting was applied to fully explore the conformational space. GA Calculations were performed for 200 times. GoldScore was chosen to assess the binding affinity. The best binding conformations were used for further analysis. In post-docking analysis, 2D and surface plots were prepared by Maestro 9.4.

4.5. Molecular dynamics and MM-GBSA

System building: The docked conformation of the **I-14**-proteasome complex was used in the molecular dynamics study. The complex was solved in TIP3P water model with a concentration of NaCl of 0.15 mol/L. The box size calculation method was set to buffer with a distance parameter of 10×10×10 Å. The solutes were reoriented to minimize the box size. Six Na^+ were added automatically to obtain an electrically neutral system. OPLS_2005 forcefield was used to build the system. Minimization: The model system is minimized by using a hybrid method of the steepest decent and the limited-memory Broyden-Fletcher-Goldfrab-Shanno (LBFGS) algorithms with maximum iterations at 2000 and convergence threshold at 1.0 kcal/mol/Å. Molecular Dynamics: The total simulation time was set to 30.0 ns with a trajectory interval of 4.8 ps. The default NPT ensemble relaxation protocol was performed before the simulation. The final unrestrained simulation was carried out at a constant pressure (1.01325 bar) and temperature (300.0 K). Post-processing: The representative conformation for 10–30 ns was analyzed and acquired in an interval of 10 steps. MM-GBSA: **I-14** and the receptor was splited and saved into different files before the calculation to cater to the needs of the MM-GBSA module in Prime (Schrödinger LLC.). Thus the total binding free energy (ΔG_{bind}) of the molecule with the covalent binding energy can't be given. For different frames from the simulation, we used the VSGB solvation model with OPLS_2005 forcefield and minimized polar hydrogens

ACCEPTED MANUSCRIPT

only to calculate the non-bonding fragments' ΔG_{bind}.

Acknowledgments

This work was financially supported by the grants from the Ministry of Science and Technology of China (2013ZX09103-001-018) and National Natural Science Foundation of China (81172915).

References

[1] (a) A. Ciechanover, The ubiquitin−proteasome proteolytic pathway. Cell. 79 (1994), 13−21; (b) R. W. King, R. J. Deshies, J. M. Peters, M. W. Kieschner, How proteolysis drives the cell cycle. Science. 274 (1996), 1652-1659; (c) A. Ciechanover, The ubiquitin-proteasome pathway: on protein death and cell life. EMBO J. 17 (1998), 7151−7160.

[2] (a) S. Y. Fuchs, The role of ubiquitin−proteasome pathway in oncogenic signaling. Cancer Biol. Ther. 1 (2002), 337−341; (b) D. Ron, P. Walter, Signal integration in the endoplasmic reticulum unfolded protein response. Nature Rev. Mol. Cell Biol. 8 (2007), 519−529; (c) J. J. Chen, F. Lin, Z. H. Qin, The roles of the proteasome pathway in signal transduction and neurodegenerative diseases. Neurosci. Bull. 24 (2008), 183−194; (d) S. S. Vembar, J. L. Brodsky, One step at a time: endoplasmic reticulum-associated degradation. Nature Rev. Mol. Cell Biol. 9 (2008), 944−957.

[3] (a) J. Adams, The proteasome: a suitable antineoplastic target. Nature Rev. Cancer. 4 (2004) 349−360; (b) E. M.Huber, M. Groll, Inhibitors for the immuno- and constitutive proteasome: current and future trends in drug development. Angew. Chem., Int. Ed. 51 (2012), 8708−8720; (c) D. L. Buckley, C. M. Crews, Small-Molecule Control of Intracellular Protein Levels through Modulation of the Ubiquitin Proteasome System. Angew. Chem., Int. Ed. 53 (2014), 2312-2330.

[4] (a) T. Hideshima, P. Richardson, D. Chauhan, V. J. Palombella, P. J. Elliott, J. Adams, K. C. Anderson, The Proteasome Inhibitor PS- 341 Inhibits Growth, Induces Apoptosis, and Overcomes Drug Resistance in Human Multiple Myeloma Cells. Cancer Res. 61 (2001), 3071−3076; (b) R. C. Kane, A. T. Farrell, R. Sridhara, R. Pazdur, United States Food and Drug Administration approval summary: bortezomib for the treatment of progressive multiple myeloma after one prior therapy. Clin. Cancer Res. 12 (2006), 2955−2960; (c) R. C. Kane, R. Dagher, A. Farrell, C. W. Ko, R. Sridhara, R. Justice, R. Pazdur, Bortezomib for the treatment of mantle cell lymphoma. Clin. Cancer Res. 13 (2007), 5291−5294.

[5] (a) B. D. Dorsey, M. Iqbal, S. Chatterjee, E. Menta, R. Bernardini, A. Bernareggi, P. G. Cassara, G. D'Arasmo, E. Ferretti, M. S. De, A. Oliva, G. Pezzoni, C. Allievi, I. Strepponi, B. Ruggeri, M. A. Ator, M. Williams, J. P. Mallamo, Discovery of a potent, selective, and orally active proteasome inhibitor for the treatment of cancer. J. Med. Chem. 51 (2008), 1068−1072; (b) E. Gallerani, M. Zucchetti, A first in human phase I study of the proteasome inhibitor CEP-18770 in patients with advanced solid tumours and multiple myeloma. Eur. J. Cancer. 49 (2013), 290-296.

[6] (a) Food US, Administration D. Approved Drugs − Carfilzomib. **2012**. Available from: http://www.fda.

ACCEPTED MANUSCRIPT

gov/Drugs/InformationOnDrugs/ApprovedDrugs/ucm312945.htm; (b) K. Fostier, A. De Becker, R. Schots, Carfilzomib: a novel treatment in relapsed and refractory multiple myeloma. Onco Targets Ther. 5 (2012), 237-244; (c) D. S. Siegel, T. Martin, M. Wang, R. Vij, A. J. Jakubowiak, S. Lonial, S.Trudel, V. Kukreti, N. Bahlis, M. Alsina, A. Chanan-Khan, F. Buadi, F. J. Reu, G. Somlo, J. Zonder, K. Song, A. K. Stewart, E. Stadtmauer, L. Kunkel, S. Wear, A. F. Wong, R. Z. Orlowski, S. Jagannath, A phase 2 study of single-agent carfilzomib (PX-171-003- A1) in patients with relapsed and refractory multiple myeloma. Blood. 120 (2012), 2817−2825.

[7] (a) S. Omura, K. Matsuzaki, T. Fujimoto, K. Kosuge, T. Furuya, S. Fujita, A. Nakagawa, New microbial metabolite which induces differentiation of neuroblastoma cells. J. Antibiot. 44 (1991), 117-118; (b) P. C. Hogan, E. J. Corey, Proteasome inhibition by a totally synthetic β-Lactam related to Salinosporamide A and Omuralide. J. Am. Chem. Soc. 127, (2005) 15386−15387; (c) C. A. P. Joazeiro, K. C. Anderson, T. Hunter, Hunter proteasome inhibitor drugs on the rise. Cancer Res. 66 (2006), 7840-7842.

[8] (a) D. Chen, M. Frezza, S. Schmitt, J. Kanwar, Q. P. Dou, Bortezomib as the first proteasome inhibitor anticancer drug: current status and future perspectives. Curr. Cancer Drug Targets. 11 (2011), 239−253; (b) A. Allegra, A. Alonci,; D. Gerace, S. Russo, V. Innao, L. Calabrò, C. Musolino, New orally active proteasome inhibitors in multiple myeloma. Leukemia Research. 38 **(2014)**, 1-9.

[9] Roemmele, R. Caroline, WO 2011/087822 A1.

[10] D. Nix, C. Pien, R. Newman, T. Madden, E. Felix, J. Adams, P. Elliott, Clinical development of a proteasome inhibitor, PS-341, for the treatment of cancer. Proc. Am. Soc. Clin. Oncol. 20 (2001), 86a.

[11] (a) T. A. Lansdell, M. A. Hurchla, J. Xiang, S. Hovde, K. N. Weilbaecher, R. W. Henry, J. J. Tepe, Noncompetitive modulation of the proteasome by imidazoline scaffolds overcomes bortezomib resistance and delays MM tumor growth in vivo. ACS Chem. Biol. 8 (2013), 578−587; (b) L. M. Azevedo, T. A. Lansdell, J. R. Ludwig, R. A. Mosey, D. K. Woloch, D. P. Cogan, G. P. Patten, M. R. Kuszpit, J. S. Fisk, J. J. Tepe, Inhibition of the human proteasome by imidazoline scaffolds. J. Med. Chem. 56 (2013), 5974−5978; (c) S. Kawamura, Y. Unno, A. List, A. Mizuno, M. Tanaka, T. Sasaki, M. Arisawa, A. Asai, M. Groll, S. Shuto, Potent proteasome inhibitors derived from the unnatural cis-cyclopropane isomer of belactosin A: synthesis, biological activity, and mode of action. J. Med. Chem. 56 (2013), 3689−3700; (d) Z. Miller, K. S. Kim, D. M. Lee, V. Kasam, S. E. Baek, K. H. Lee, Y. Y. Zhang, L.Ao, K. Carmony, N. R. Lee, S. Zhou, Q. Zhao, Y. Jang, H. Y. Jeong, C. G. Zhan, W. Lee, D. E. Kim, K. B. Kim, Proteasome inhibitors with pyrazole scaffolds from structure-based virtual screening. J Med Chem. 58 (2015), 2036-2041.

[12] B. D. Dorsey, M. Iqbal, Discovery of a potent, selective, and orally active proteasome inhibitor for the treatment of cancer. J. Med. Chem. 51 (2008), 1068-1072.

[13] B. D. Dorsey, M. Iqbal, S. Chatterjee, E. Menta, R. Bernardini, A. Bernareggi, P. G. Cassarà, G. D Arasmo, E. Ferretti, S. De Munari, A. Oliva, G. Pezzoni, C. Allievi, I. Strepponi, B. Ruggeri, M. A. Ator, M. Williams, J. P. Mallamo, Discovery of a potent,

ACCEPTED MANUSCRIPT

selective, and orally active proteasome inhibitor for the treatment of cancer. J. Med. Chem. 51 (2008), *51*, 1068-1072.
[14] Y. Q. Zhu, S. Y. Yao, B. Xu, Z. M. Ge, J. R. Cui, T. M. Cheng, R. T. Li, Design, synthesis and biological evaluation of tripeptide boronic acid proteasome inhibitors. Bioorg. Med. Chem. 17 **(2009)**, 6851-6861.
[15] M. Lei, X. Zhao, Z. Wang, Y. Q. Zhu, Pharmacophore modeling, docking studies, and synthesis of novel dipeptide proteasome inhibitors containing boron atoms. J. Chem. Inf. Model. 49 (2009), 2092-2100.
[16] Y. Q. Zhu, X. R. Zhu, G. Wu, Y. H. Ma, Y. J. Li, X. Zhao, Y. X. Yuan, J. Yang, S. Y. Yu, F. Shao, R. T. Li, Y. R. Ke, A. J. Lu, Z. M. Liu, L. R. Zhang, Synthesis, in vitro and in vivo biological evaluation, docking studies, and structure−activity relationship (SAR) discussion of dipeptidyl boronic acid proteasome inhibitors composed of β-amino acids. J. Med. Chem. 53 (2010), 1990-1999.
[17] S. Kawamura, Y. Unno, A. Asai, M. Arisawa, S. Shuto, Structurally novel highly potent proteasome inhibitors created by the structure-based hybridization of nonpeptidic Belactosin derivatives and peptide boronates. J. Med. Chem. 57 (2014), 2726-2735.
[18] J. Clerc, B. Schellenberg, M. Groll, Convergent synthesis and biological evaluation of syringolin A and derivatives as eukaryotic 20S proteasome inhibitors. Eur. J. Org. Chem. 21 (2010), 3991-4003.
[19] J. Clerc, M. Groll, D. J. Illich, A. S. Bachmann, R. Huber, B. Schellenberg, R. Dudler, M. Kaiser, Synthetic and structural studies on syringolin A and B reveal critical determinants of selectivity and potency of proteasome inhibition. Proc. Natl. Acad. Sci. U. S. A. 106 (2009), 6507-6512.
[20] W. A. Van der Linden, L. I. Willems, T. B. Shabaneh, N. Li, M. Ruben, B. I. Florea, G. A. van der Marel, M. Kaiser, A. F. Kisselev, H. S. Overkleeft, Discovery of a potent and highly beta1 specific proteasome inhibitor from a focused library of urea-containing peptide vinyl sulfones and peptide epoxyketones. Org. Biomol. Chem. 10 (2012), 181-194.
[21] P. A. Duspara, M. S. Islam, A. J. Lough, R. A. Batey, Synthesis and reactivity of N-alkyl carbamoylimidazoles: development of N-methyl carbamoylimidazole as a methyl isocyanate equivalent. J. Org. Chem. 77 (2012), 10362-10368.
[22] A. B. Melissa, Chihui, A. E. Jonathan, Asymmetric copper-catalyzed synthesis of α-amino boronate esters from N-tert-butanesulfinyl aldimines. J. Am. Chem. Soc. 130 (2008), 6910-6911.
[23] (a) J. Sun, M. T. Perfetti, W. L. Santos, A method for the deprotection of alkylpinacolyl boronate esters. J. Org. Chem. 76 (2011), 3571-3575; (b) R. C. Roemmele, M. A. Christie, Development and Scale-Up of an Optimized Route to the Peptide Boronic Acid, CEP-18770. Org. Process Res. Dev. 17 (2013), 422-426.
[24] L. J. Milo, J. H. Lai, W. Wu, Y. Liu, H. Maw, Y. Li, Z. Jin, Y. Shu, S. E. Poplawski, Y. Wu, D. G. Sanford, J. L. Sudmeier, W. W. Bachovchin, Chemical and Biological Evaluation of Dipeptidyl Boronic Acid Proteasome Inhibitors for Use in Prodrugs and Pro-Soft Drugs Targeting Solid Tumors. J. Med. Chem. 54 (2011), 4365-4377.

ACCEPTED MANUSCRIPT

[25] L. Lemoucheux, J. Rouden, M. Ibazizene, F. Sobrio, M. Lasne, Debenzylation of tertiary amines using phosgene or triphosgene: An efficient and rapid procedure for the preparation of carbamoyl chlorides and unsymmetrical ureas. Application in Carbon-11 chemistry. J. Org. Chem. 68 (2003), 7289-7297.
[26] (a) J. Yang, Z. Wang, Y. Fang, J. Jiang, F. Zhao, H. Wong, M. K. Bennett, C. J. Molineaux, C. J. Kirk, Pharmacokinetics, pharmacodynamics, metabolism, distribution, and excretion of carfilzomib in rats. Drug Metab. Dispos. 39 (2011), 1873−1882; (b) V. Uttamsingh, C. Lu, G. Miwa, L. S. Gan, Relative contributions of the five major human cytochromes P450, 1A2, 2C9, 2C19, 2D6, and 3A4, to the hepatic metabolism of the proteasome inhibitor bortezomib. Drug Metab. Dispos. 33 (2005), 1723−1728; (c) M. Hasegawa, Y. Yasuda, M. Tanaka, K. Nakata, E. Umeda, Y. Wang, C. Watanabe, S. Uetake, T. Kunoh, M. Shionyu, R. Sasaki, I. Shiina, T. Mizukami, A novel tamoxifen derivative, ridaifen-F, is a nonpeptidic small-molecule proteasome inhibitor. Eur. J. Med. Chem. 71 (2014), 290-305.
[27] A. F. Kisselev, W. A. Van der Linden, H. S. Overkleeft, Proteasome inhibitors: an expanding army attacking a unique target. Chem Biol. 19 (2012), 99-115.
[28] A. Julian, Preclinical and clinical evaluation of proteasome inhibitor PS-341 for the treatment of cancer. Curr Opin Chem Biol. 6 (2002), 493–500.

ACCEPTED MANUSCRIPT

ACCEPTED MANUSCRIPT

Table of Contents

ACCEPTED MANUSCRIPT

ACCEPTED MANUSCRIPT

Highlights

• Two series of novel urea-containing peptide boronic acids were designed and synthesized as proteasome inhibitors.
• The structure-activity relationship was investigated and one of the two series showed impressive anti-proteasome and anti-tumor activities.
• More human tumor cell lines were tested and compound **I-14** was selected to evaluate its anticancer activity in vivo.
• Compound **I-14** showed obvious in vivo anticancer activity with much lower toxicity comparing to Bortezomib.

ACCEPTED MANUSCRIPT